Supplementary Information

Covalent conductive polymer chain and organic ligand ethylenediamine modified MXene-like-{$AlW_{12}O_{40}$} compounds for fully symmetric supercapacitors, electrochemical sensors and photocatalysis mechanisms

Li-Ge Gong[a], Xian-Xian Qi[a], Kai Yu[a*], Jia-Qian Gao[a], Bai-Bin Zhou[a*], Guo-Yu Yang[b*]

We successfully synthesized two kinetically stable the covalent polymer chains and ethylenediamine acting MXene-like-{$AlW_{12}O_{40}$} compounds. According to the results of energy storage research, these materials show high capacitance performance and cycle stability. The capacitors of **1-**CC(carbon cloth) and **2-**CC are 478.41 and 625.99F g^{-1}(1.0 A g^{-1}), and the capacitance retention are 95.71% and 97.62% after 5000 cycles. The symmetrical water system supercapacitor device is assembled with two **2-**CC and the energy density of 6.32Wh kg^{-1} at 237W kg^{-1}. Meanwhile, compounds **1-2** were used to test the new sensitive current hydrogen peroxide sensor, display that the linear ranges are 1.20-3.20mM(**1-**GCE:glassy carbon electrode) and 19.95μM-0.90mM(**2-**GCE) with the detection limit of 0.93μM, 0.86μM. In addition, the photocatalysis mechanisms of compounds **1-2** were studied to provide a powerful basis for the photocatalytic mechanism of this series of compounds.

Table of Contents

1. Experimental Procedures

1.1 Materials and general methods

All chemicals were commercially purchased and used without further purification. Elemental analyses (C, H, and

N) were performed on a Perkin-Elmer 2400 CHN elemental analyzer. Ag, Al, Cu and W were analyzed on a PLASMA-SPEC (I) ICP atomic emission spectrometer. The IR spectrum was recorded in the range 400-4000 cm-1 on an Alpha Centaurt FT/IR spectrophotometer using KBr pellets.The UV-vis-NIR absorption spectroscopy was measurered with a Varian Cary 500 UV-vis-NIR spectrometer. TG analyses were performed on a Perkin-Elmer TGA7 instrument with a heating rate 10 °C min^{-1}. XRD patterns were collected on Rigaku Dmax 2000 X-ray diffractometer with graphite monochromatized Cu Kα radiation (λ= 0.154 nm) and 2θ ranging from 5 to 50°. The Brunauer-Emmett-Teller (BET) surface area were performed by N_2 adsorption measurements at 77.3 K using a Nova 2000E. The scanning electron microscopy (SEM) images were measured by a Hitachi SU70 SEM coupled with an energy-dispersive X-ray (EDX) detector. X-ray photoelectron spectrum (XPS) analyses were analyzed on an AXIS ULTRA DLD electron spectrometer by an Mg Kα (1253.6 eV) achromatic X-ray source. The electrochemical measurement was carried out on a CHI660E electrochemical workstation at room temperature. The liquid chromatography was analyzed on Agilent 1260. (Condition: wondasil C18 column, 4.6 mm × 150mm, 5 um, SPD-15C UV detector, 285 nm, mobile phase Vmethanol: Vwater=4 : 6, flow rate: 1.00 mL / min, injection volume: 20μL)

1.2 X-ray crystallography

Crystal datas for compounds **1** and **2** were collected at 296(2) Bruker SMART CCD detector with graphite monochromatic MoKa radiation (λ= 0.71073Å). The structures were solved by direct methods and refined by full-matrix least-squares on F_2 using the olex2 program. All the non-hydrogen atoms were refined anisotropically. All the hydrogen atoms were placed in idealized positions and refined. Crystallographic data and structure refinements for **1** and **2** were summarized in Table S1.Selected bond lengths (Å) and angles for **1** and **2** were listed in Table S2 and Table S3.

1.3 Electrode preparation and electrochemical characterization for SCs

A conventional three-electrode system was used. The working electrode was a carbon electrode (CC), a Pt wire was the counter electrode, and Ag/AgCl (3 M KCl) electrode was used as a reference electrode. The impedance spectroscopy measurement was performed on a CHI660E over the frequency range from 0.1 Hz to 1 MHz with an applied voltage of 50 mV.

The carbon cloth electrodes of compounds 1-2 : The working electrodes were made by mixing as-synthesized compound (80 wt%), PVDF (10 wt%) and acetylene black (10 wt%) in N-methyl pyrrolidinone, and grinding the compounds for about 30 min to form a slurry, which was then coated on carbon cloth (1 cm^2) and dried at 60℃ for 12 h. The weight of the as-prepared electrodes was controlled about 2~3 mg.

$$Cs = \frac{2I_m \int V dt}{V^2 \left| \frac{V_f}{V_t} \right|} \quad \text{Equation (S1)}$$

In which $I_m=I/m$, I (A) is the current for discharge, m (g) is the mass of the electrode material, t (s) is the time discharged, V (V) is the discharge potential range with final value(V_f).

Symmetric device: The solid-type supercapacitor device was constructed by two cloth electrodes in 0.5 M H_2SO_4 electrolyte with a piece of polypropylene membrane as a separator. The total active mass was 4~6 mg.

$$C_- \times m_- \times \Delta V_- = C_+ \times m_+ \times \Delta V_+$$

Equation(S2)

where C_-, C_+, m_+, m_-, ΔV_+ and ΔV_- are the specifific capacitance, mass and potential range of the negative and positive electrodes.

1.4 Photocatalysis experiments

Aqueous suspensions of RhB, MB or MO(100 mL, 10mg/L) and compounds **1** or **2** (50 mg) were placed in the vessel. Prior to irradiation, the mixed suspensions were magnetically stirred in the dark for 20 min to ensure the equilibrium of the working solution. At given time intervals, 3mL aliquots were sampled and analyzed by using a Varian Cary 500 UV-vis-NIR spectrometer. Finally, the solvent of the filtrate was removed under the reduced pressure and the crystal of 1 or 2 were retrieved.

1.5 Electrode preparation and electrochemical characterization for sensors

The working electrode was the glassy carbon electrode(GCE), a Pt wire was the counter electrode, and Ag/AgCl (3 M KCl) electrode was used as a reference electrode.

Preparation of the **1**-, **2**-GCE: Compound **1** or **2** was mixed with acetylene black as raw material and was ground into slurry in 3:1 ethanol solution. The dispersed slurry (5μL) was dripped onto the glassy carbon electrode surface to form a uniform film at room temperature for 2 hours. Then the Nafion solution (5μL) was dripped on the electrode surface as a protective film and was dried for 1 hours.

2. Results and Discussion

2.1 The structural diagrams of compounds 1-2

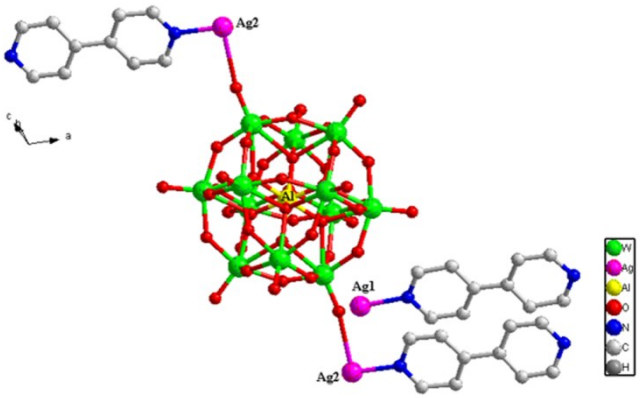

Figure S1. The ellipsoid structure of the compound **1**

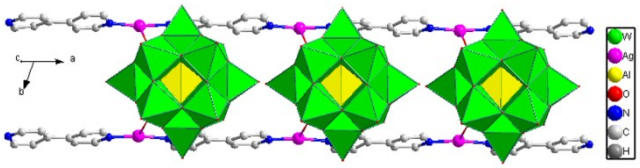

Figure S2. The 1D chain structure of the compound **1**

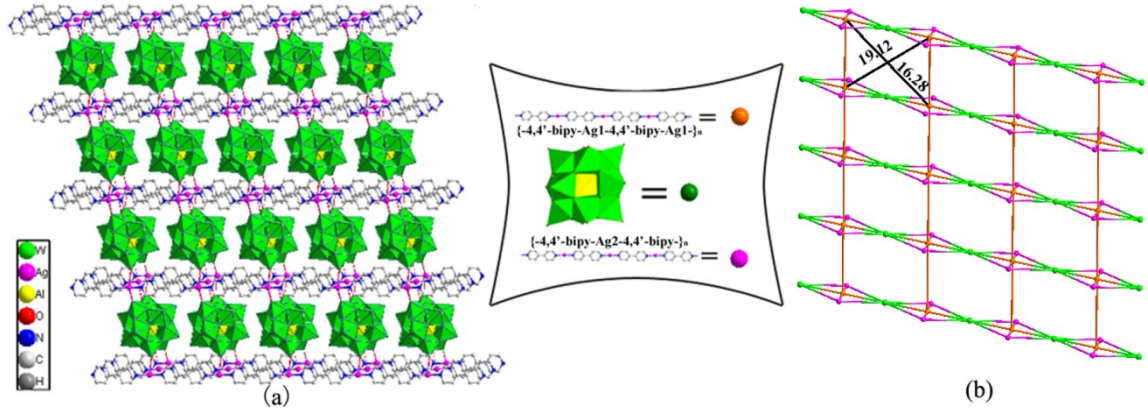

Figure S3.(a)The polyhedral and ball-and-stick view of the 2D sheet structure of compound **1**. All H atoms are omitted for clarity;(b) The 2D topology structure of compound **1**.

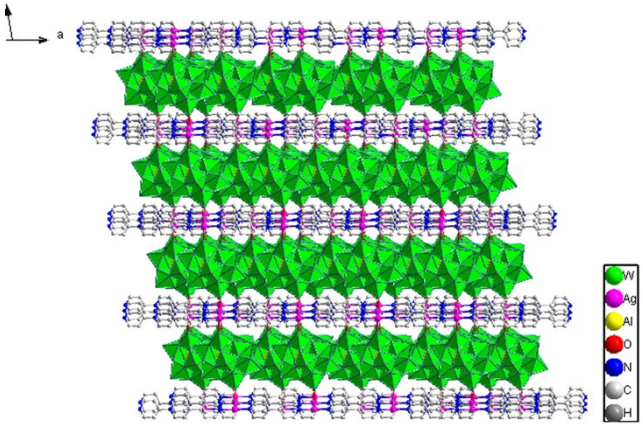

Figure S4. The 3D structure of compound **1.**

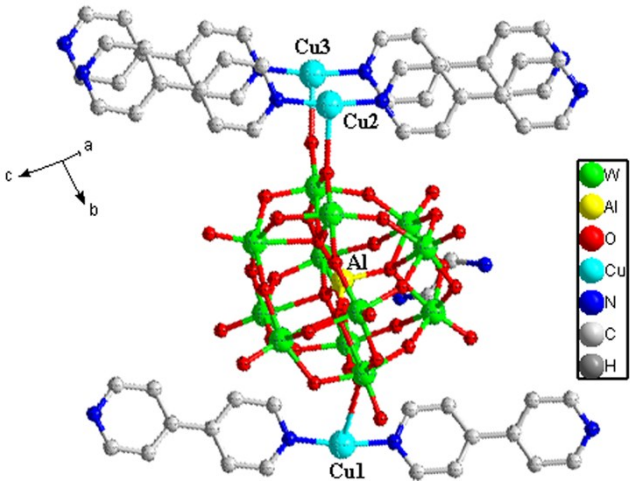

Figure S5. The ellipsoid structure of the compound **2.**

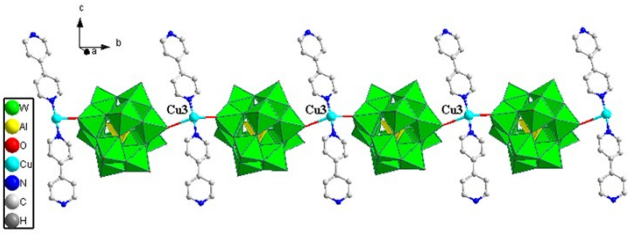

Figure S6. The 1D chain structure of the compound **2.**

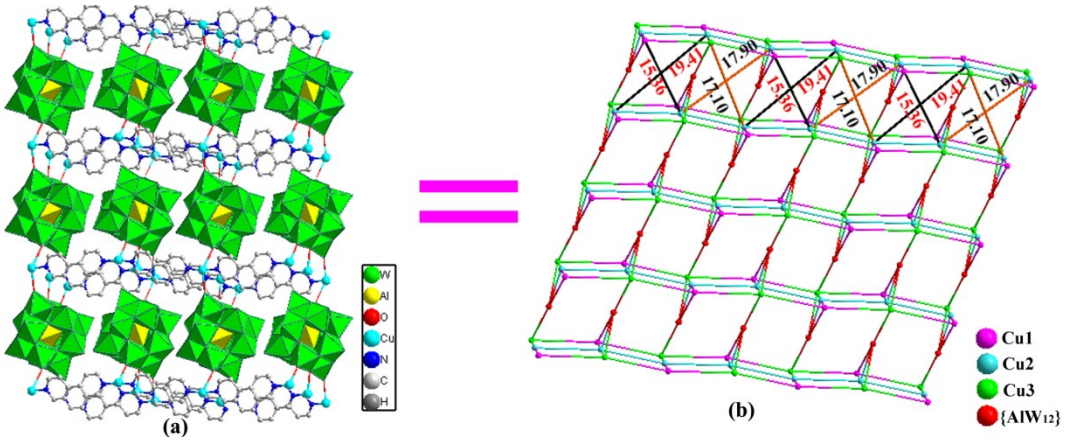

Figure S7. (a)The polyhedral and ball-and-stick view of the 2D sheet structure of compound **2**. All H atoms are omitted for clarity;(b) The 2D topology structure of compound **2**.

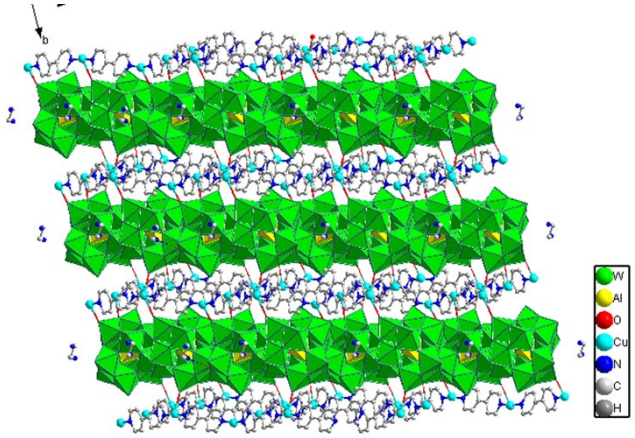

Figure S8. The 3D structure of compound **2.**

2.2 The characterization diagrams of compounds 1-2

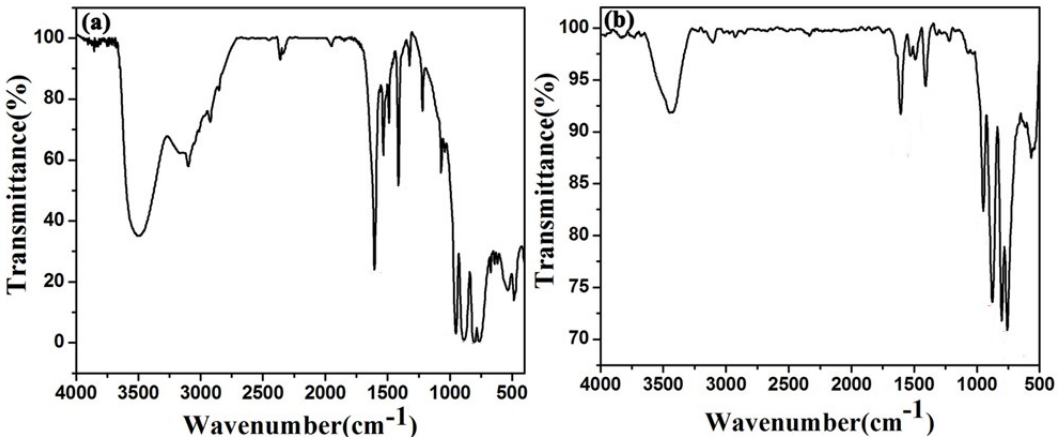

Figure S9. IR spectra of compound **1** (a) and compound **2** (b).

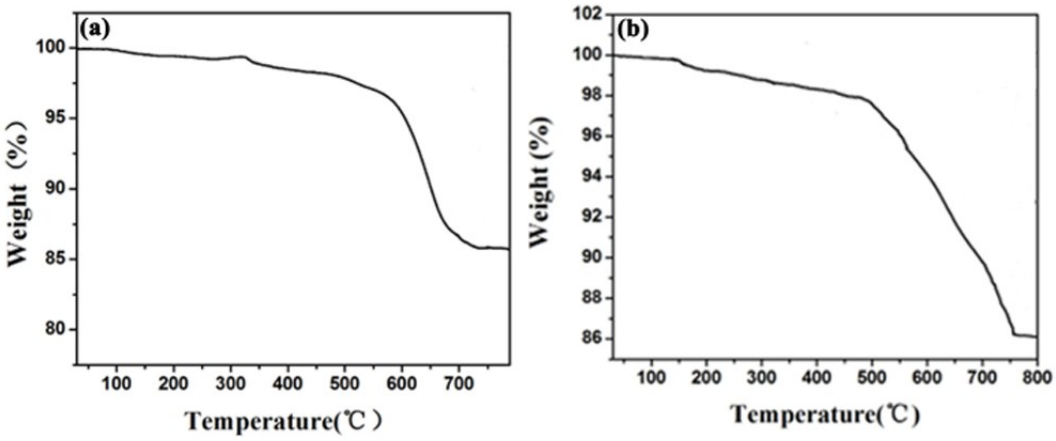

Figure S10.TG curves of compound **1** (a) and compound **2** (b).

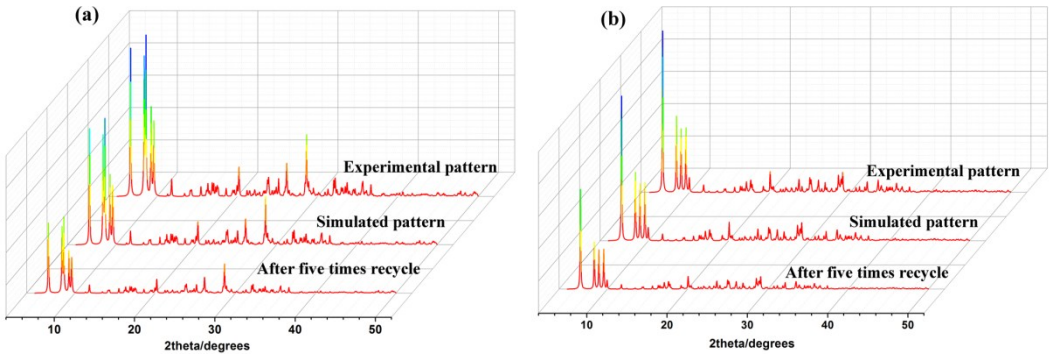

Figure S11. The XRD patterns for compound **1** (a) and compound **2** (b).

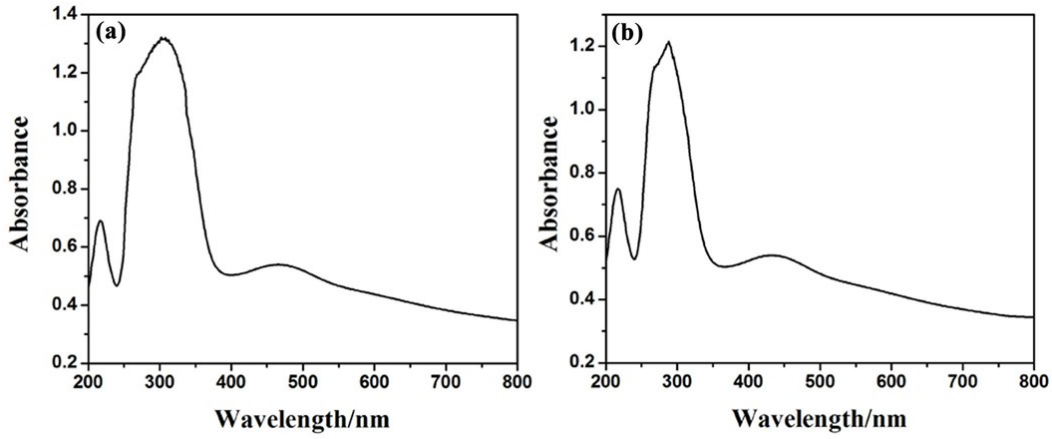

Figure S12. Solid state UV-vis spectra of compound **1** and compound **2**

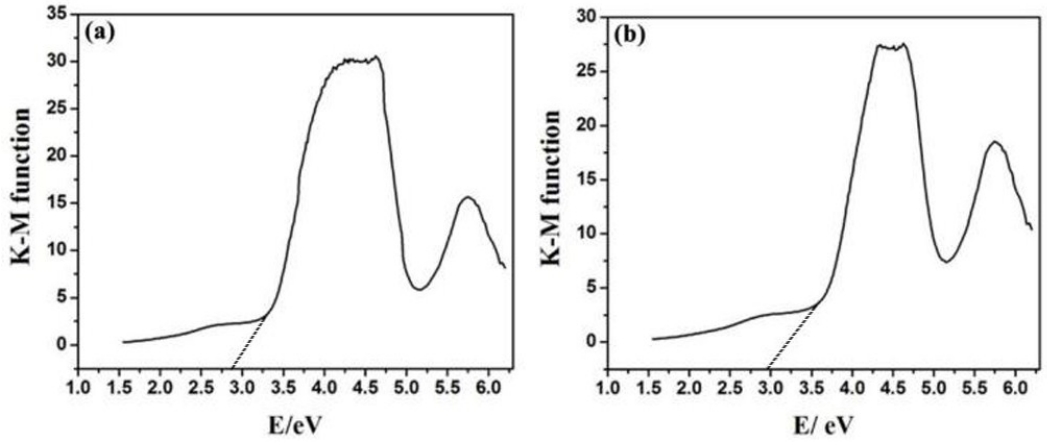

Figure S13. Kubelka-Munk transformed diffuse reflectance spectra of (a) compound **1** (b) compound **2**.

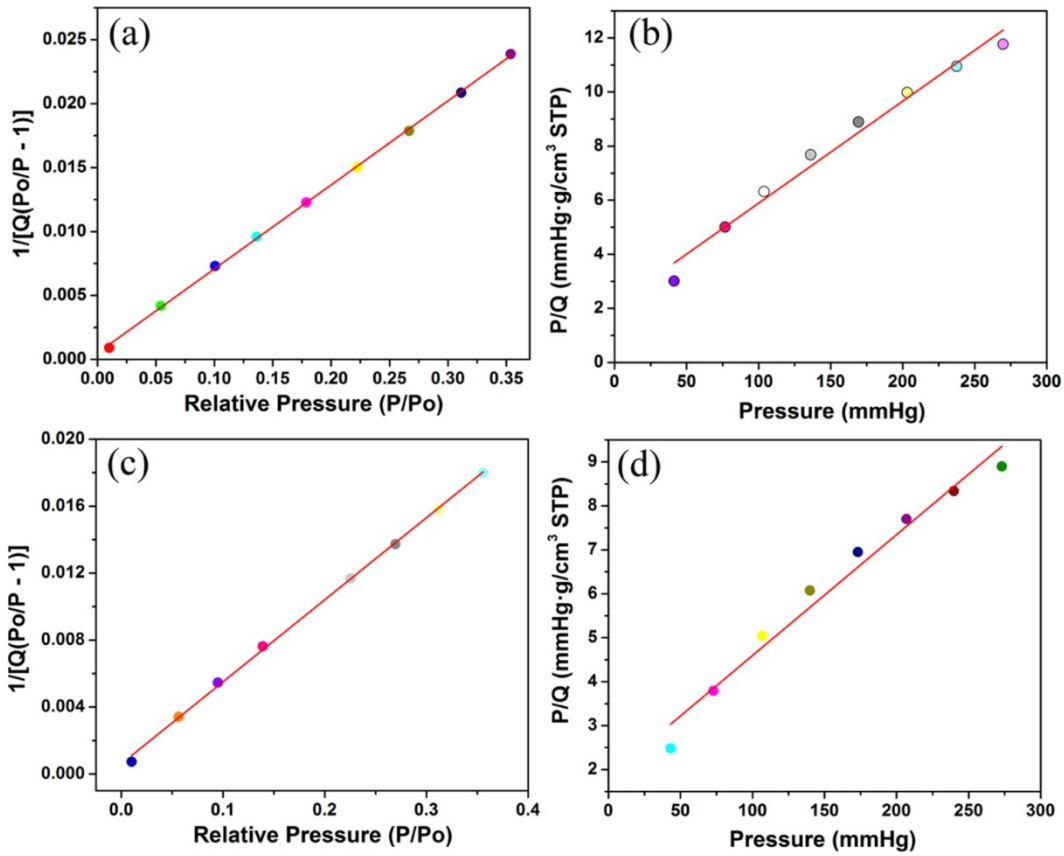

Figure S14. (a)The BET surface area for compound **1**; (b)The langmuir surface area for compound **1**; (c)The BET surface area for compound **2**; (d) The langmuir surface area for compound **2**.

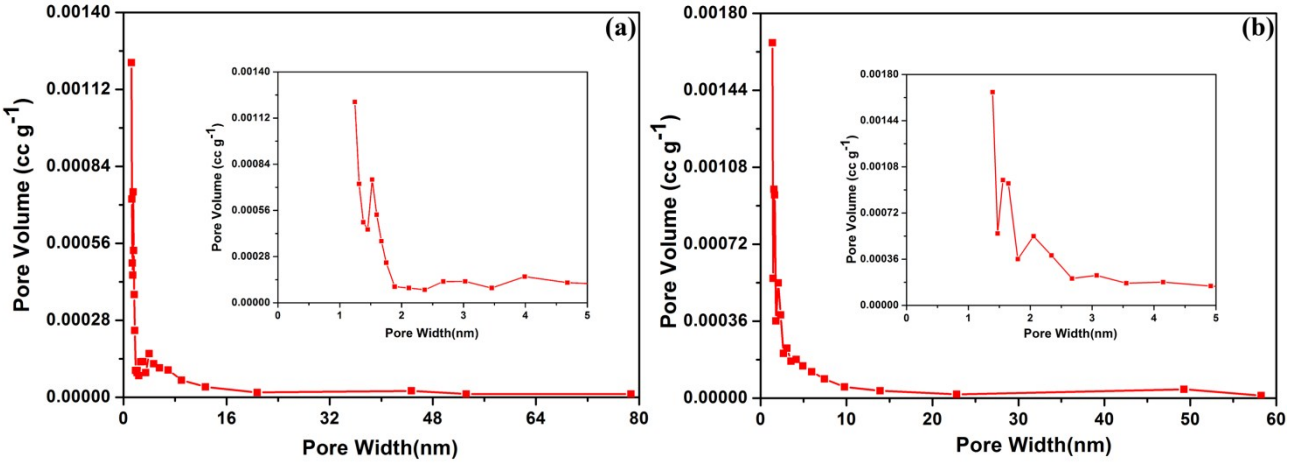

Figure S15. Pore size distribution from DFT method: (a) compound **1**; (b) compound **2**

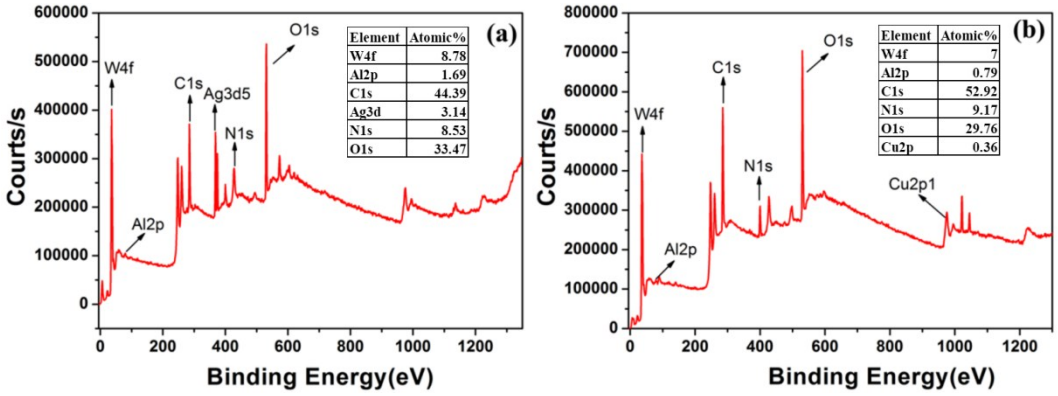

Figure S16. The XPS of compound **1**(a) and compound **2**(b).

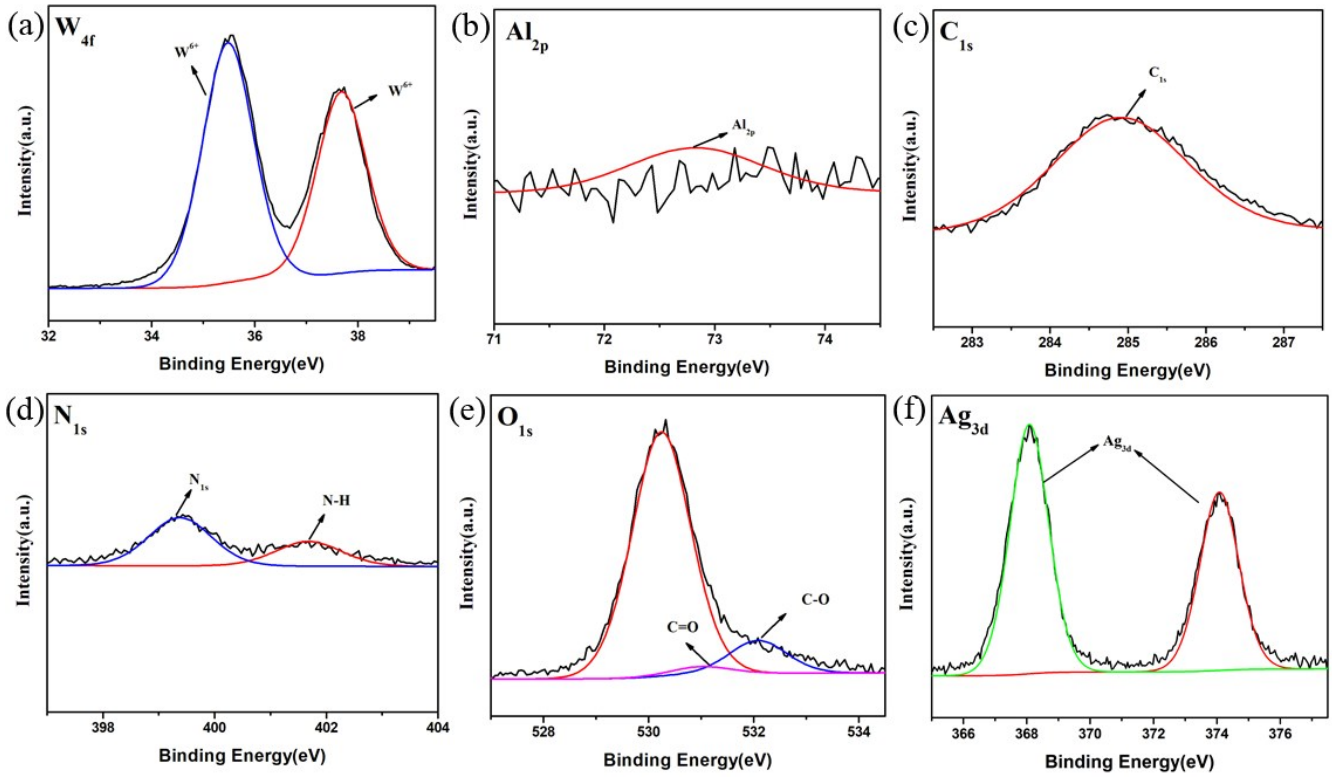

Figure S17. XPS spectra of compound **1**：(a) W4f ; (b) Al2p; (c) C1s; (d) N1s; (e) O1s; (f) Ag3d.

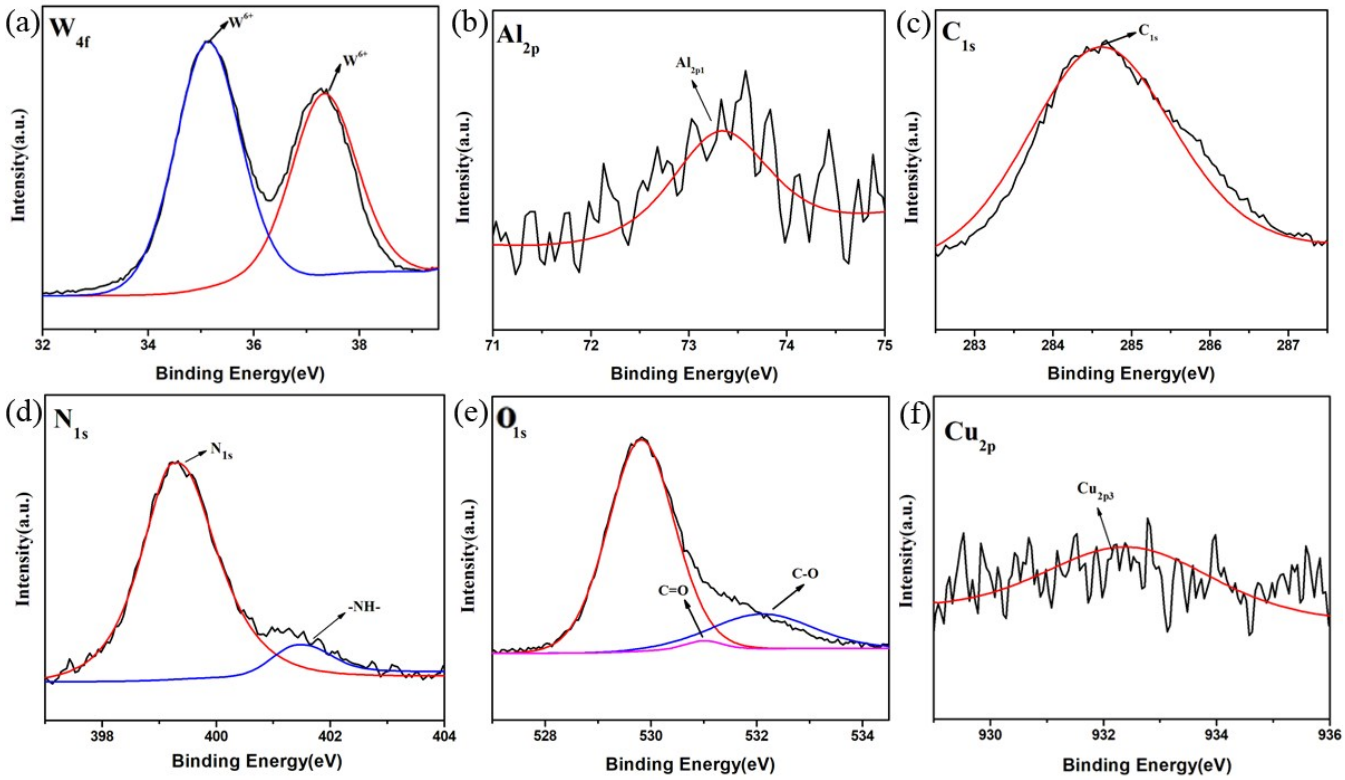

Figure S18. XPS spectra of compound **2**：(a) W4f; (b)Al2p; (c)C1s; (d) N1s; (e)O1s; (f) Cu2p.

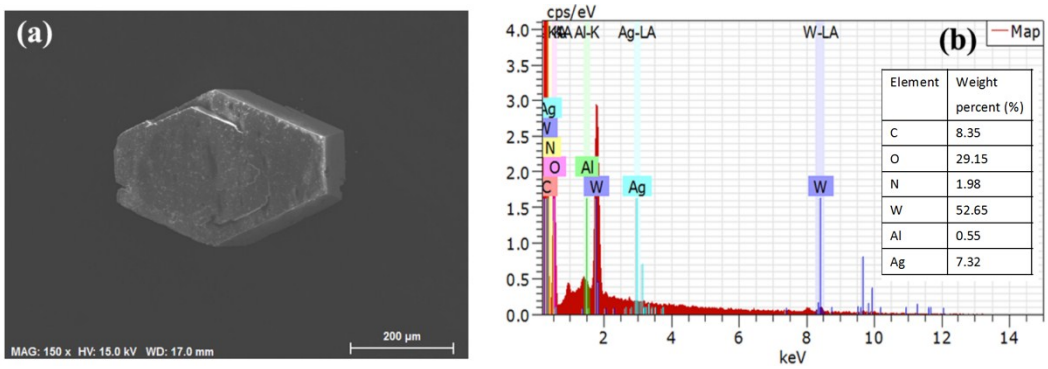

Figure S19. The SEM and EDS of compound **1**.

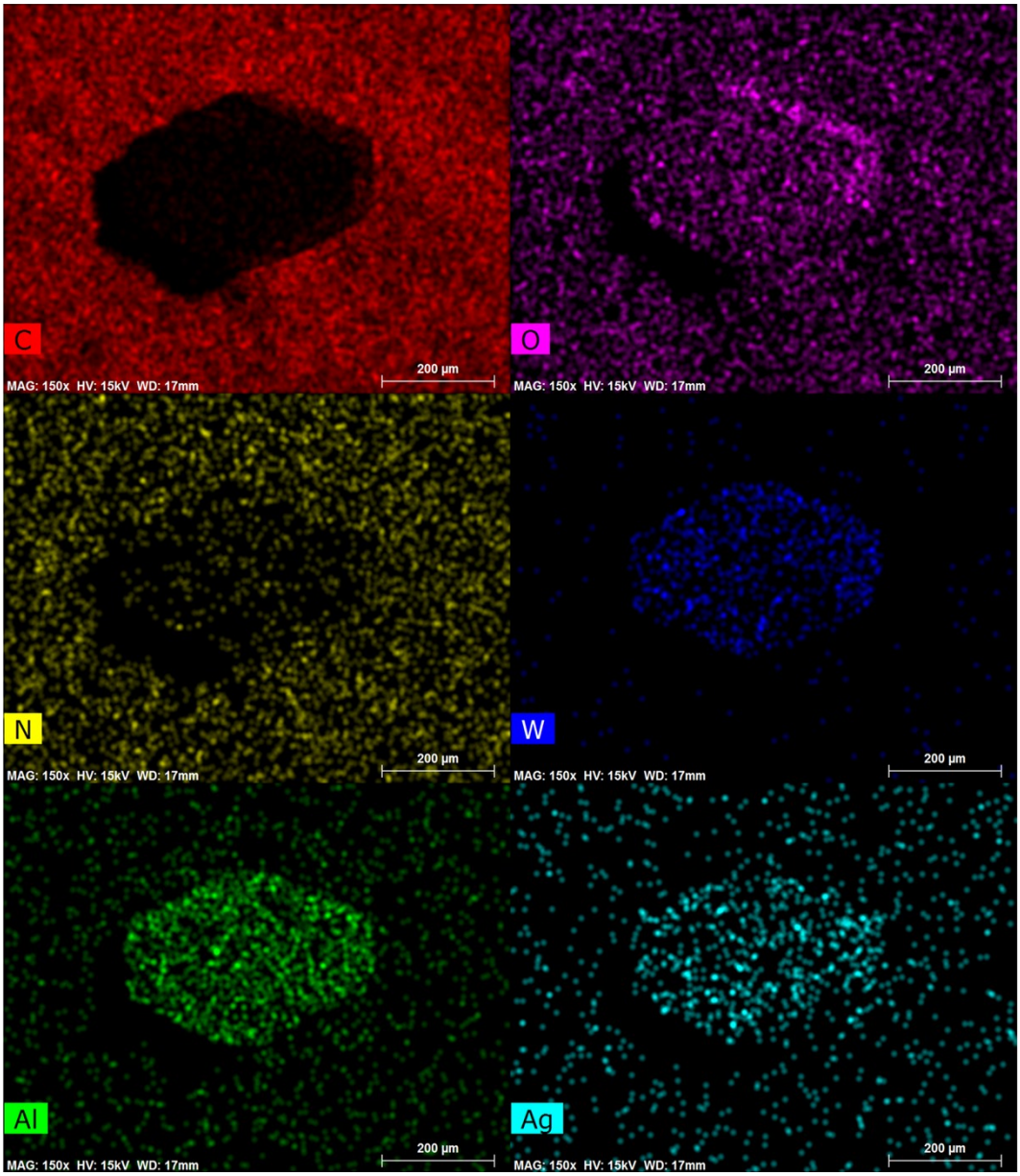

Figure S20. The mapping of compound **1**.

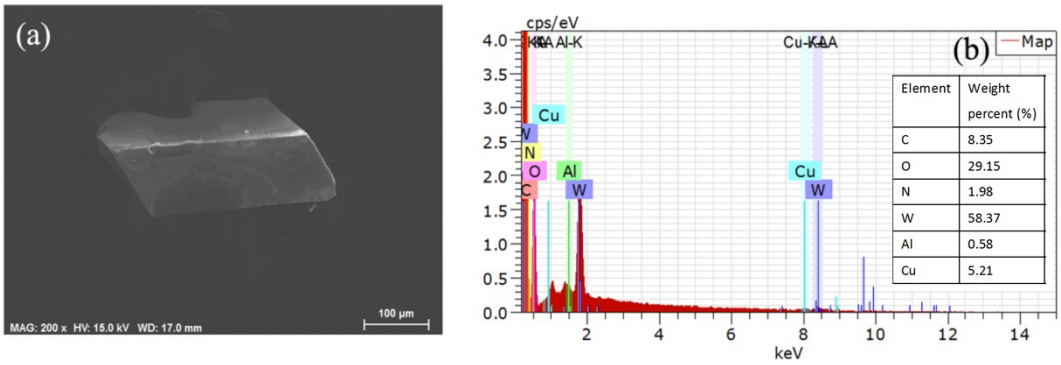

Figure S21. The SEM and EDS of compound **2**.

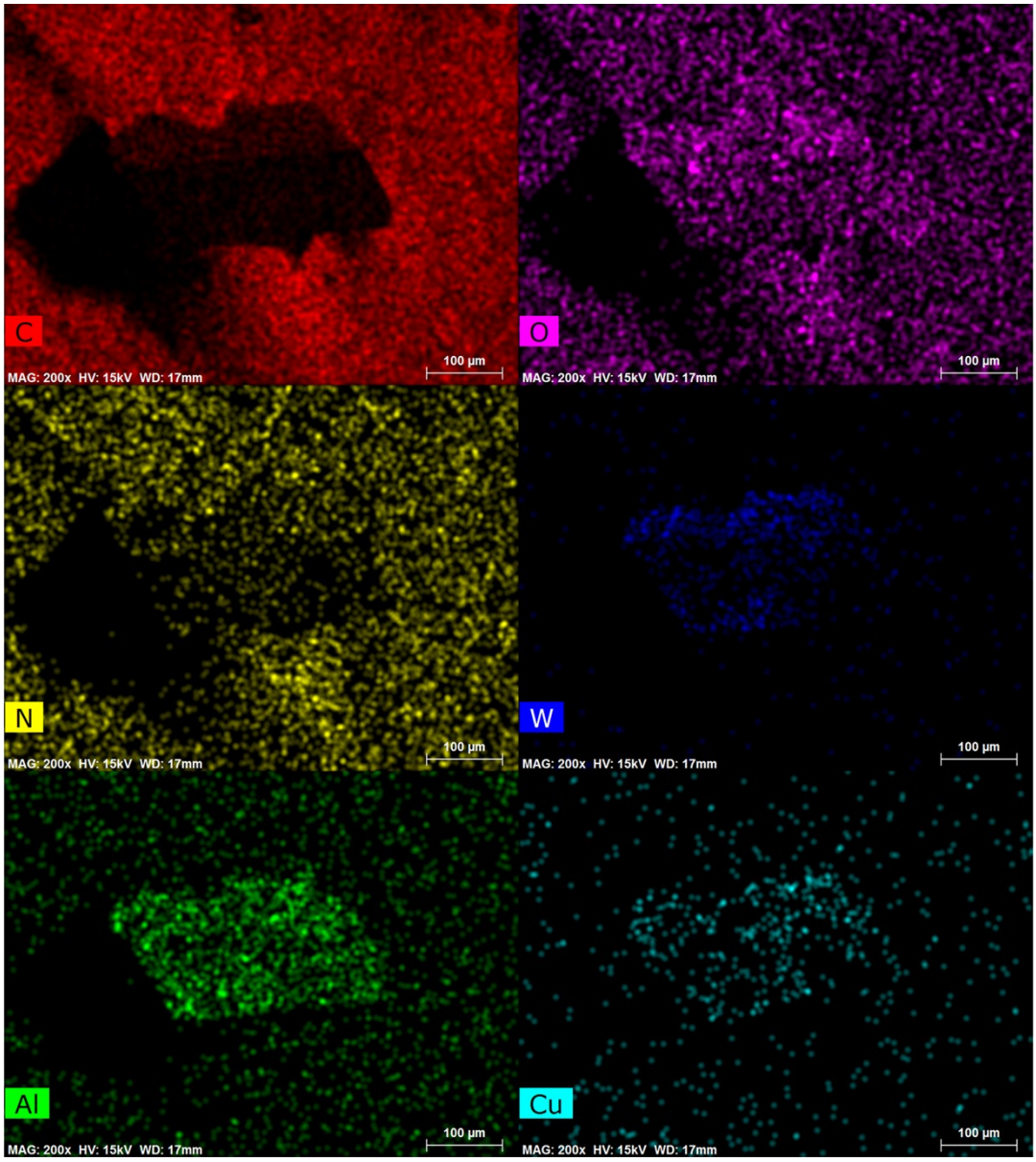

Figure S22. The mapping of compound **2**.

2.3 The supercapacitor testing diagrams of compounds 1-2

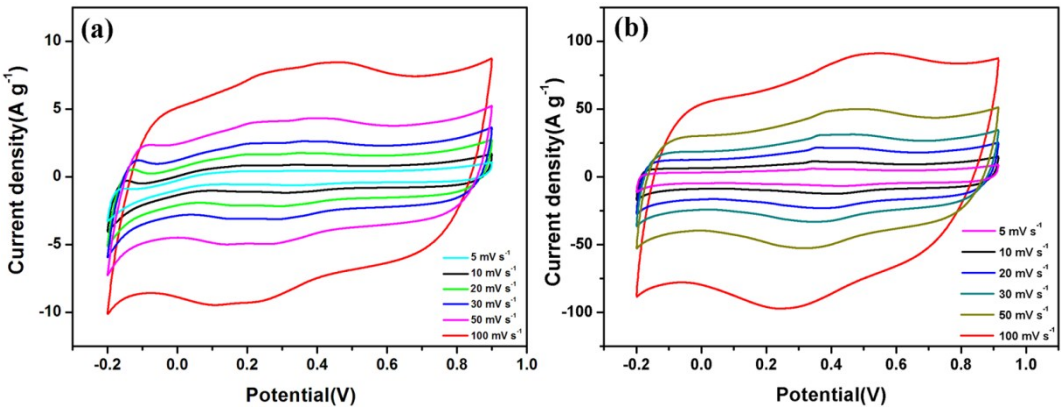

Figure S23. The CVs at different scan rates:(a) $Na_5AlW_{12}O_{40}$ (b)compound **1**.

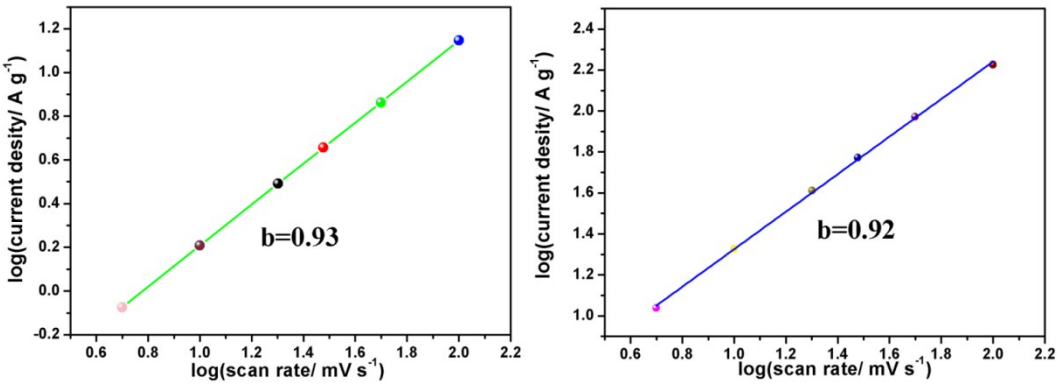

Figure S24. The b values of $Na_5AlW_{12}O_{40}$ (a) and **1**-CC (b).

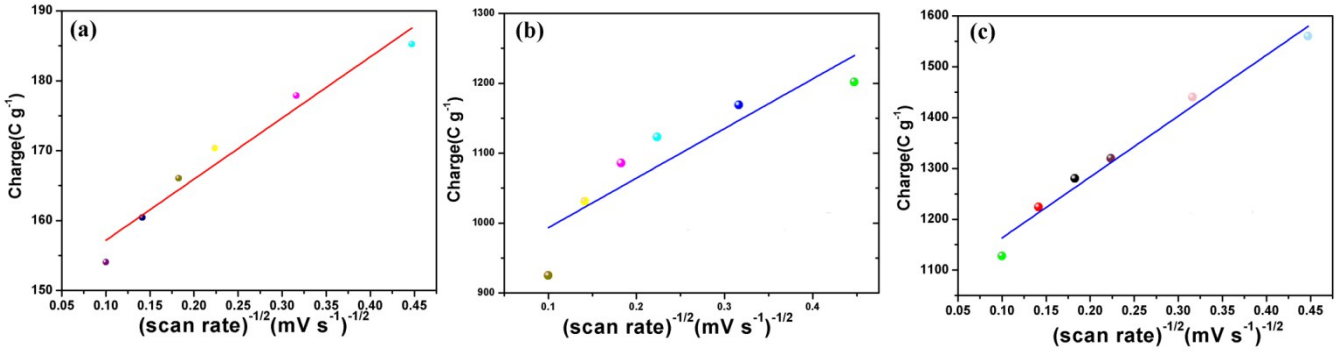

Figure S25. The linear diagram of the stored charge (q) and the square root reciprocal of the scan rate($v^{-1/2}$) for $Na_5AlW_{12}O_{40}$(a); **1**-CC(b) and **2**-CC(c).

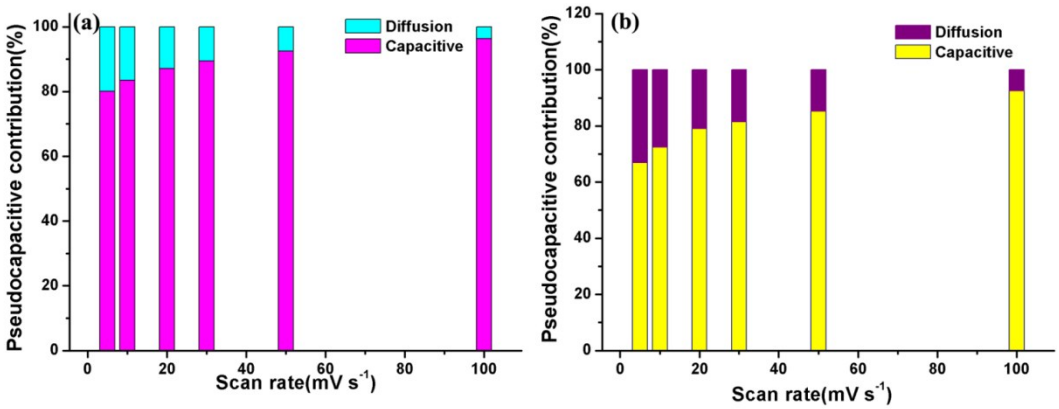

Figure S26. Q_s and Q_d are estimated for $Na_5AlW_{12}O_{40}$(a) ; **1**-CC(b)

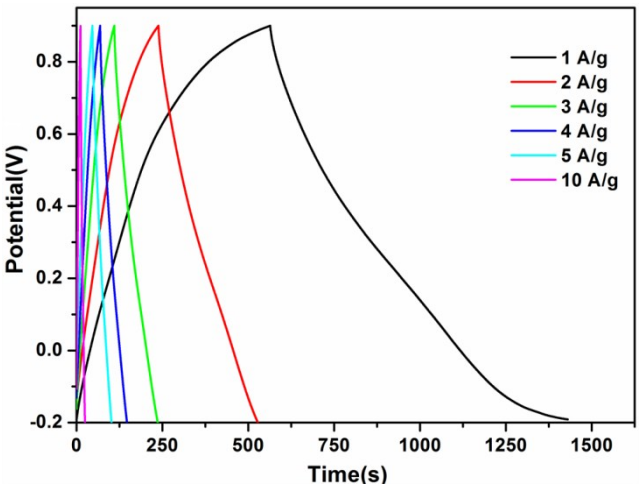

Figure S27. The GCD of **1**-CC at 1, 2 , 3 , 5 and 10 A g^{-1}.

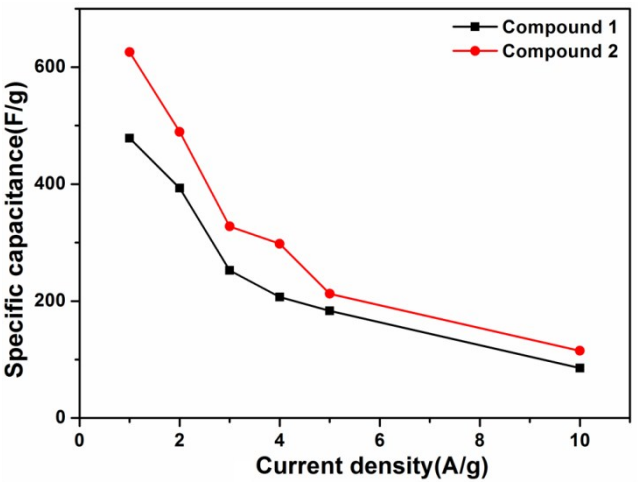

Figure S28. The good rate capability of compound **1** and compound **2**.

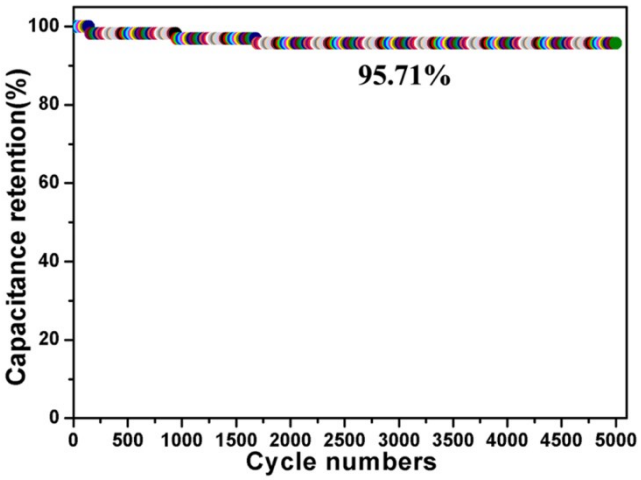

Figure S29. Cycling stability of **1**-CC after 5000 cycles.

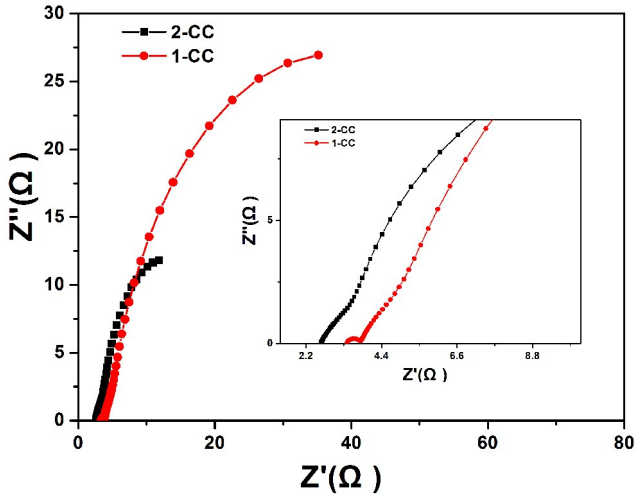

Figure S30. Impedance analysis of the **1**-CC and **2**-CC.

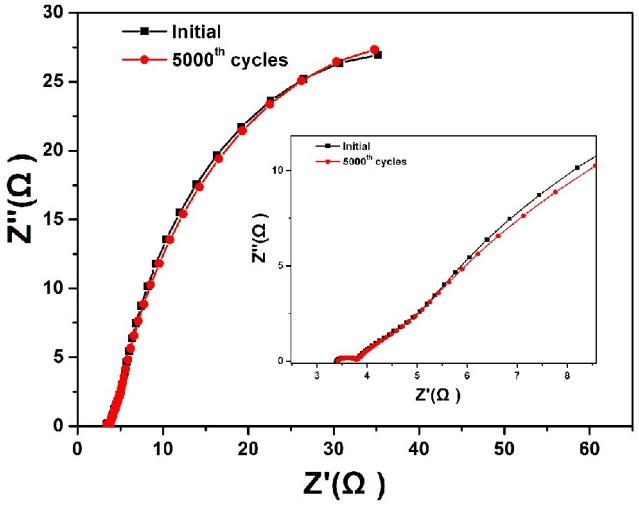

Figure S31. Impedance analysis of the **1**-CC before and after 5000 cycles.

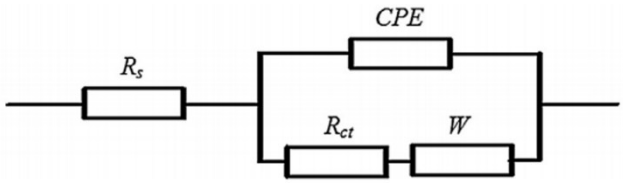

Figure S32. The equivalent circuit diagrams of EIS for 2-CC

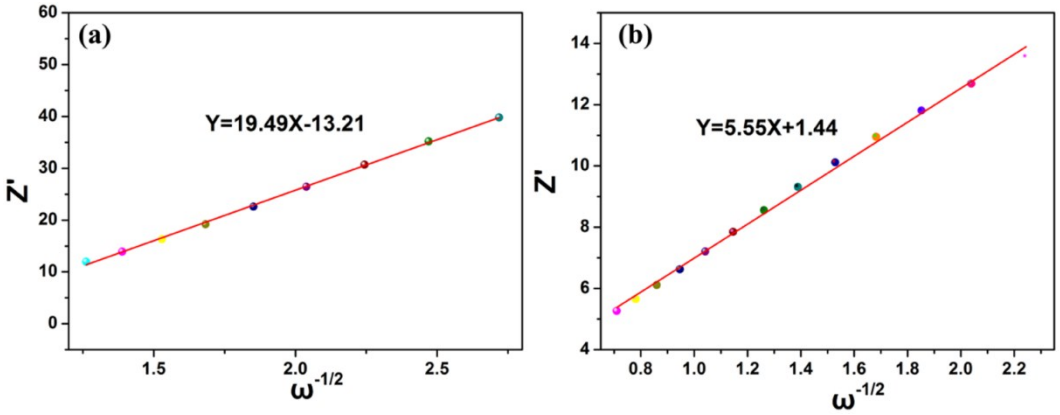

Figure S33. The linear relationship between Z' and $\omega^{-1/2}$ for compound **1** (a) and compound **2**(b).

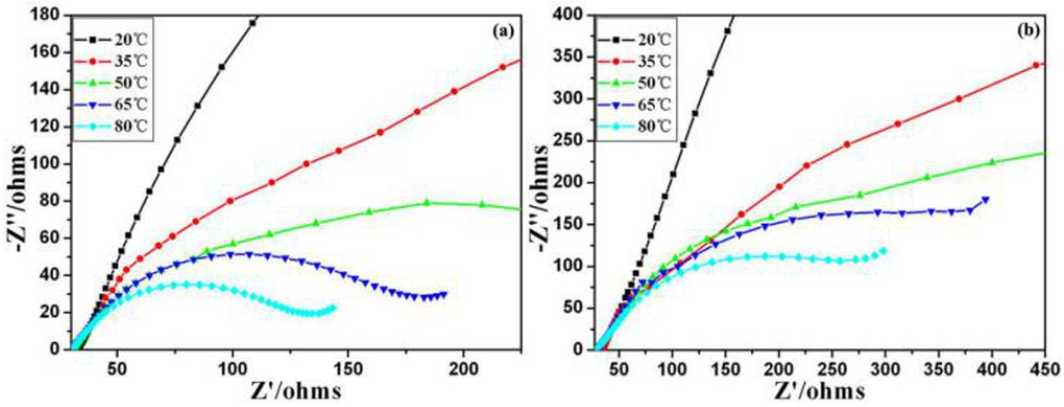

Figure S34. Nyquist plots of (a) compound **1** and (b) **2** at different temperatures.

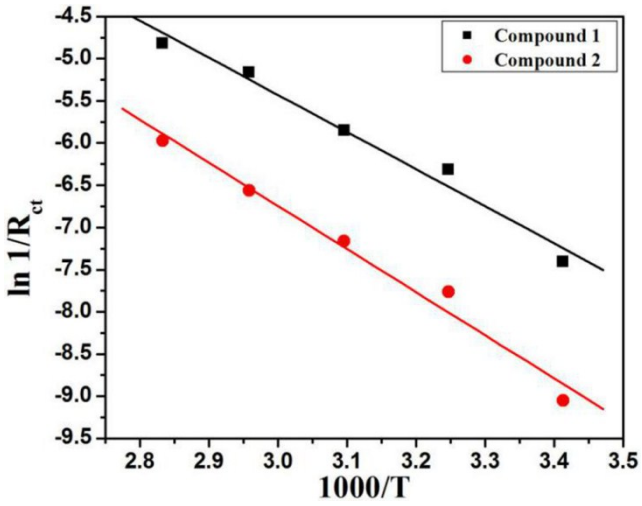

Figure S35. Arrhenius plots of (a) compound **1** and (b) compound **2**.

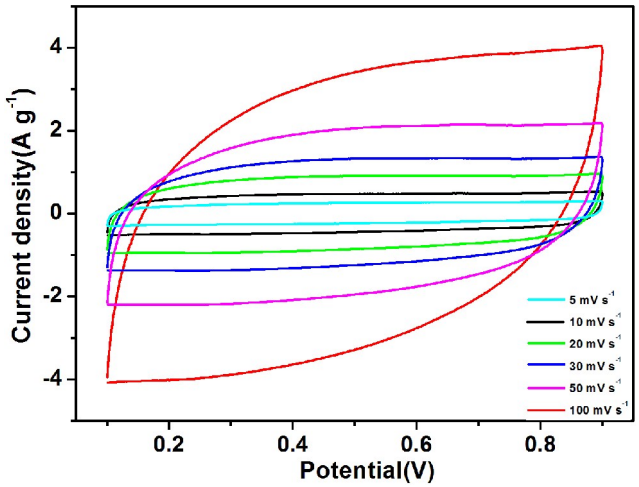

Figure S36. The CV curves for the symmetrical water system supercapacitor device.

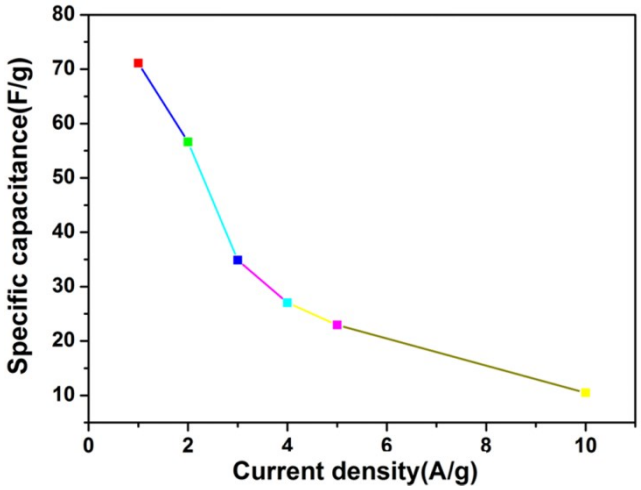

Figure S37. The good rate capability of the symmetrical water system supercapacitor device.

2.4 The photocatalytic diagrams of compounds 1-2

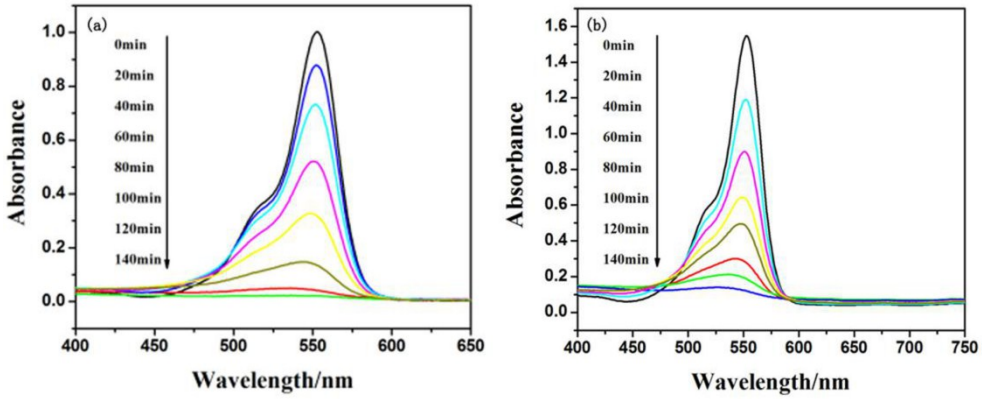

Figure S38. The photocatalysis behaviors to reduce rhodamine B (RhB) in the solution of (a) compound **1** and (b)compound **2** .

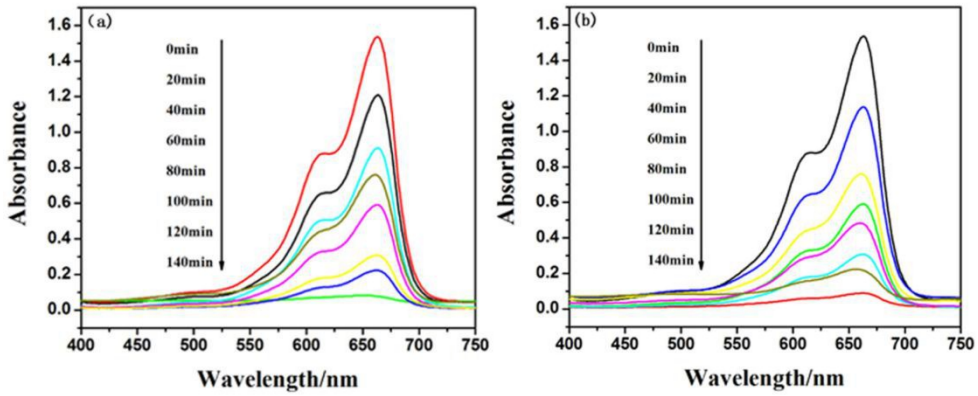

Figure S39. The photocatalysis behaviors to reduce methylene blue (MB) in the solution of (a) compound **1** and (b) compound **2**.

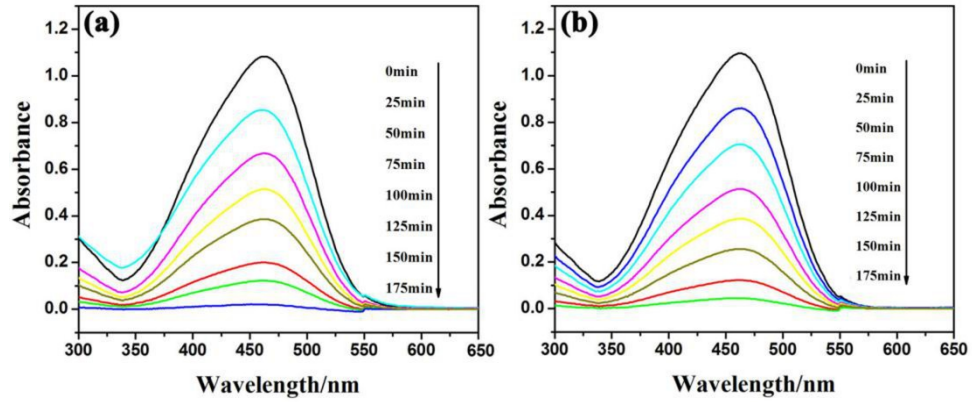

Figure S40. The photocatalysis behaviors to reduce methylene blue (MO) in the solution of (a) compound **1** and (b)compound **2**.

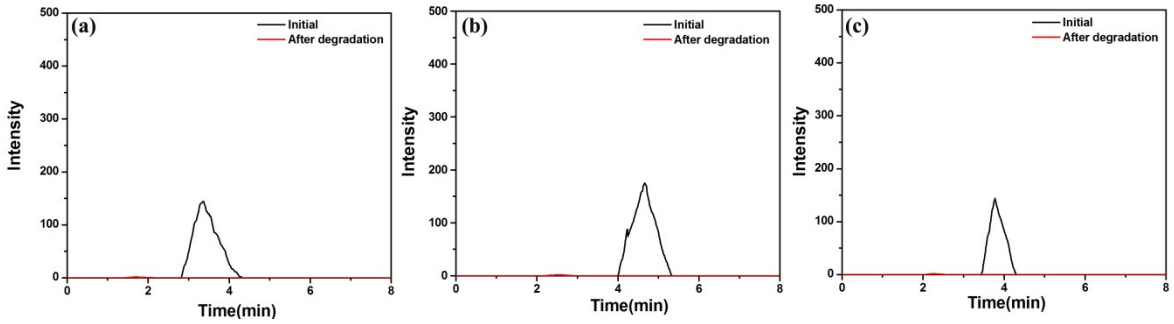

Figure S41. The samples before and after dye degradation were analyzed by liquid chromatography(LC): (a) MB (b) RhB (c) MO

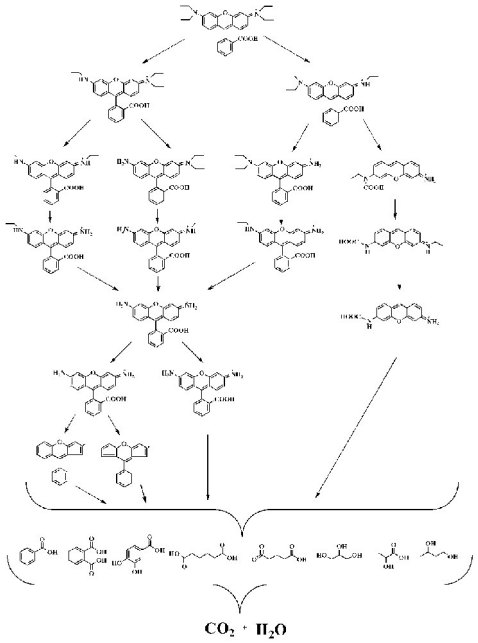

Figure S42. The possible degradation mechanism of RhB[1].

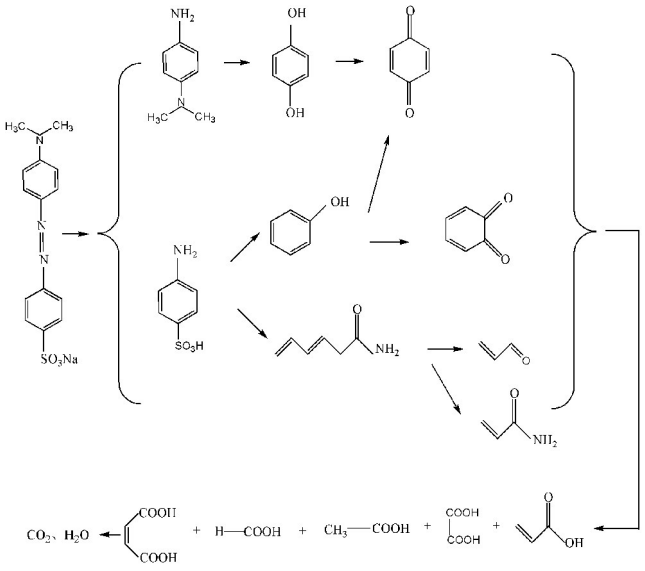

Figure S43. The possible degradation mechanism of MO[2].

2.5 The electrocatalytic diagrams of compounds 1-2

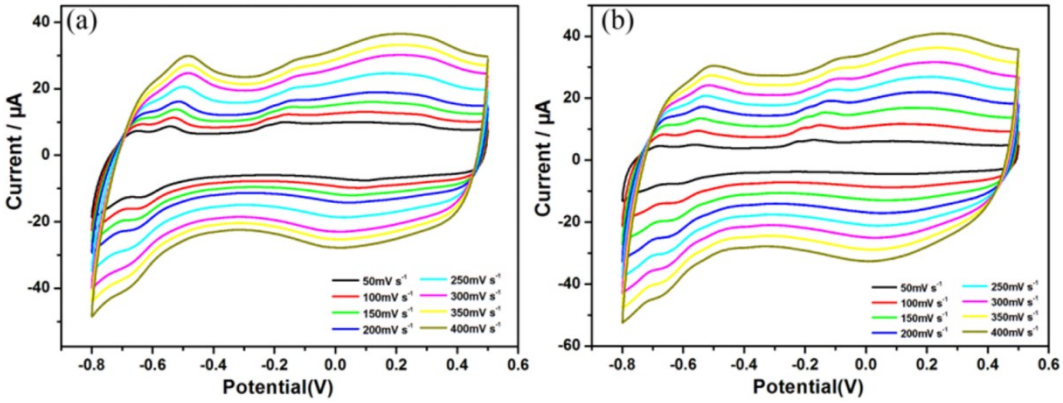

Figure S44. The CVs in a 0.1M H_2SO_4 + 0.5M Na_2SO_4 aqueous solution at different scan rates in the potential range from -0.8 to 0.5 V: (a) **1**-GCE (b) **2**-GCE.

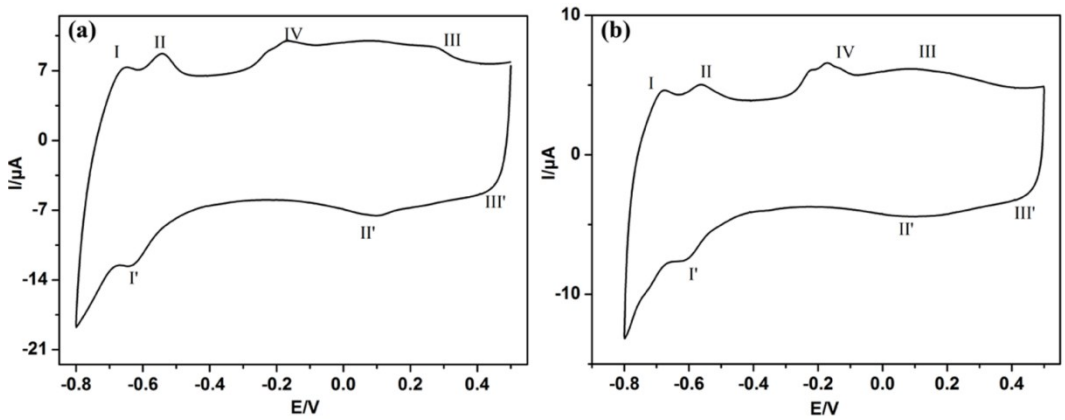

Figure S45. The CVs of **1**-GCE(a) and **2**-GCE(b) at 50mVs^{-1}.

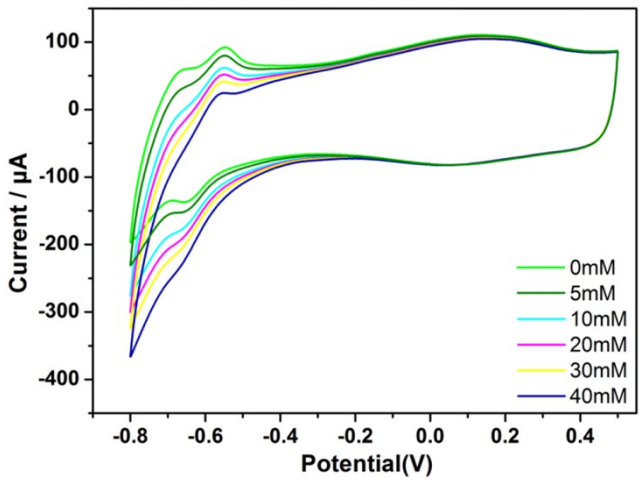

Figure S46. Reduction of H_2O_2 at **1**-GCE(Scan rate: 50mVs^{-1}).

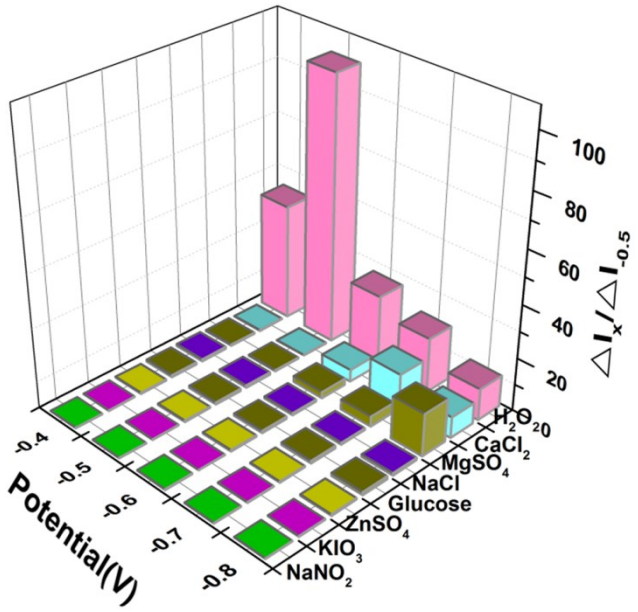

Figure S47. The selectivity profile of compound **1** at -0.4~ -0.8V.

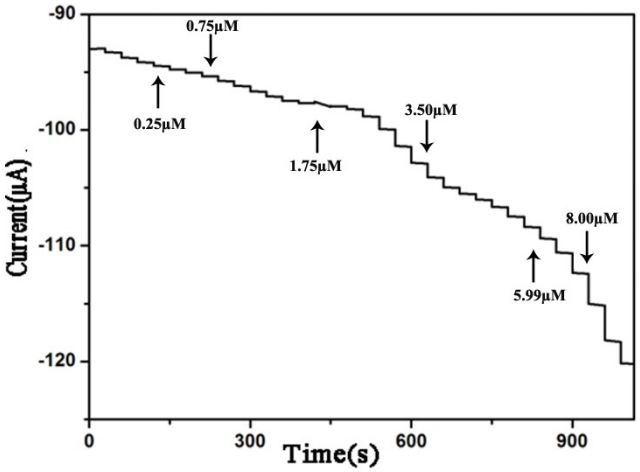

Figure S48. The i-t curve of compound **1** with successive additions of H_2O_2

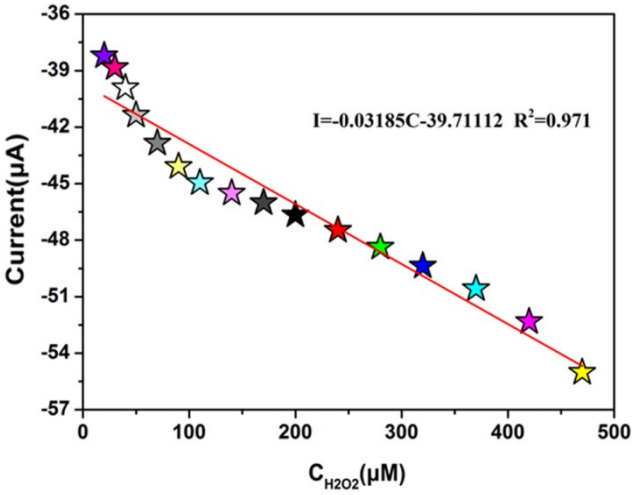

Figure S49. The linear relationship between the current response of compound **1** and the concentration of H_2O_2.

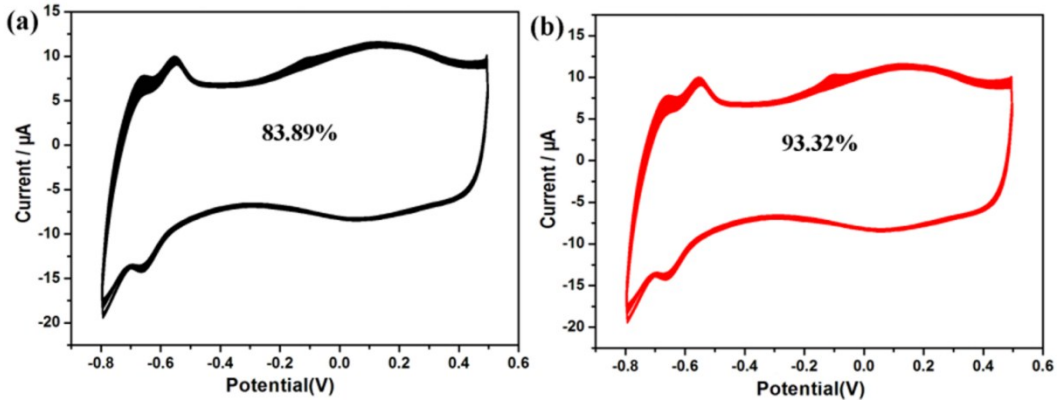

Figure S50. The CVs of 1000 cycles at a 50 m V s^{-1} (a) compound 1 (b) compound **2**

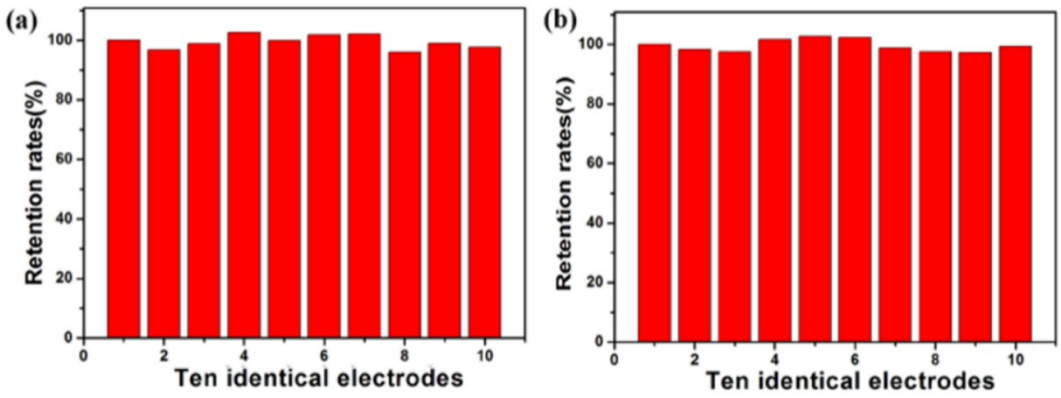

Figure S51. The reproducibility of **1**-GCE(a) and **2**-GCE(b).

2.6 Crystal data and structure refinements for compounds 1-2

Table S1. Crystal data and structure refinements for compounds **1-2**.

Compound	**1**	**2**
Formula	C30H24Ag3AlN6O41W12	C32H34Cu3AlN8O43W12
Mr	3729.22	3642.38
Crystal system	Triclinic	Triclinic
Space group	P1	P -1
a, Å	11.361(3)	12.6484(3)
b, Å	11.614(4)	13.7085(3)
c, Å	13.645(4)	18.5245(4)
α, deg	97.533(3)	89.671(1)
β, deg	99.346(2)	85.9080(10)
γ, deg	112.178(2)	75.421(1)
V, Å^3	1608.2(8)	3100.38(12)
Z	1	2
Crystal size	0.14×0.12×0.11	0.13×0.13×0.12
Dcalcd, Kg m^{-3}	3.851	3.902
μ(MoKα), mm^{-1}	22.361	23.282
F(000), e	1640.0	3228.0
θ range, deg/°	2.67-27.42	2.54 -27.51
Reflections collected	17328	34725
Data/restraints/parameters	7254/ 594 /437	14218 / 0 / 894
R_1/wR_2	0.1176 / 0.1437	0.0331/ 0.0724
GoF on F^2	1.040	1.047

$^a R_1 = \Sigma||Fo| - |Fc||/\Sigma|Fo|$; $^b wR_2 = \Sigma[w(Fo^2 - Fc^2)^2]/[w(Fo^2)^2]^{1/2}$.

2.7 Table of bond lengths and bond angles for compounds 1-2

Table S2. Selected bond lengths (Å) and angles for compound **1**.

W(1)-O(1)	1.86(4)	W(1)-O(2)	1.64(3)	W(1)-O(3)	1.94(4)

W(1)-O(4)	1.86(3)	W(1)-O(5)	2.41(4)	W(1)-O(16)	2.31(4)
W(1)-O(18)	1.76(4)	W(2)-O(3)	1.85(4)	W(2)-O(5)	2.22(3)
W(2)-O(10)	1.86(3)	W(2)-O(13)	1.67(3)	W(2)-O(14)	2.32(3)
W(2)-O(15)	1.78(3)	W(2)-O(17)	1.91(4)	W(3)-O(4)	1.90(3)
W(3)-O(5)	2.27(3)	W(3)-O(6)	1.94(3)	W(3)-O(8)	1.68(3)
W(3)-O(9)	2.27(3)	W(3)-O(10)	1.91(3)	W(3)-O(12)	1.87(3)
W(4)-O(6)	1.88(3)	W(4)-O(7)	1.67(3)	W(4)-O(9)	2.25(3)
W(4)-O(11)	1.87(3)	W(4)-O(14)	2.26(4)	W(4)-O(15)	1.94(3)
W(4)-O(22)	1.92(4)	W(5)-O(1)	1.90(4)	W(5)-O(14)	2.36(4)
W(5)-O(16)	2.22(4)	W(5)-O(17)	1.85(4)	W(5)-O(20)	1.82(4)
W(5)-O(21)	1.68(3)	W(5)-O(22)	1.89(3)	W(6)-O(9)	2.41(4)
W(6)-O(11)	1.87(3)	W(6)-O(12)	1.88(3)	W(6)-O(16)	2.25(3)
W(6)-O(18)	1.93(4)	W(6)-O(19)	1.69(3)	W(7)-O(20)	1.90(3)
Al(1) -O(5)	1.78(3)	Al(1) -O(9)	1.76(3)	Al(1) -O(14)	1.76(3)
Al(1)-O(16)	1.84(3)	Ag(1)-O(3)	3.18(4)	Ag(1)-N(1)	2.11(3)
Ag(1)-N(1)	2.11(3)	Ag(2)-O(2)	2.65(3)	Ag(2)-N(2)	2.14(3)
Ag(2)-N(3)	2.11(3)				
O(2)-W(1)-O(1)	103(2)	O(2)-W(1)-O(3)	98.3(18)	O(2)-W(1)-O(4)	104.3(16)
O(2)-W(1)-O(5)	151.7(15)	O(2)-W(1)-O(16)	150.5(14	O(2)-W(1)-O(18)	100.0(18)
O(13)-W(2)-O(3)	103.1(19)	O(13)-W(2)-O(5)	157.4(16	O(13)-W(2)-O(10)	102.3(14)
O(13)-W(2)-O(14)	151.0(17)	O(13)-W(2)-O(15)	101.6(15	O(13)-W(2)-O(17)	99(2)
O(8)-W(3)-O(4)	98.1(19)	O(8)-W(3)-O(4)	151.6(17	O(8)-W(3)-O(6)	99.2(16)
O(8)-W(3)-O(9)	156.5(16)	O(8)-W(3)-O(10)	101.9(16	O(8)-W(3)-O(12)	106.6(19)
O(7)-W(4)-O(6)	98.3(14)	O(7)-W(4)-O(9)	153.9(15	O(7)-W(4)-O(11)	100.7(18)
O(7)-W(4)-O(14)	155.3(15)	O(7)-W(4)-O(15)	105.4(14	O(7)-W(4)-O(22)	102.1(18)
O(21)-W(5)-O(1)	100.2(19)	O(21)-W(5)-O(14)	150.5(16	O(21)-W(5)-O(16)	154.7(17)
O(21)-W(5)-O(17)	101.0(18)	O(21)-W(5)-O(20)	105.1(17	O(21)-W(5)-O(22)	97.5(16)
O(19)-W(6)-O(9)	149.7(15)	O(19)-W(6)-O(11)		O(19)-W(6)-O(12)	99.8(16)
O(19)-W(6)-O(16)	155.0(15)	O(19)-W(6)-O(18)	108.1(18	O(19)-W(6)-O(20)	103.8(17)
O(14)-Al(1)-O(5)	112.0(16)	O(14)-Al(1)-O(9)	113.2(16	O(14)-Al(1)-O(16)	108.9(17)

Table S3. Selected bond lengths (Å) and angles for compound **2**.

W(1)-O(4)	2.254(5)	W(1)-O(10)	1.959(6)	W(1)-O(15)	1.868(6)
W(1)-O(17)	1.930(5)	W(1)-O(20)	1.937(5)	W(1)-O(23)	1.717(6)
W(2)-O(1)	1.908(5)	W(2)-O(6)	2.224(5)	W(2)-O(12)	1.923(5)
W(2)-O(27)	1.870(6)	W(2)-O(31)	1.715(6)	W(2)-O(34)	1.961(6)
W(3)-O(1)	1.918(5)	W(3)-O(4)	2.249(5)	W(3)-O(8)	1.931(6)
W(3)-O(10)	1.883(6)	W(3)-O(14)	1.950(5)	W(3)-O(17)	1.711(6)
W(4)-O(2)	1.889(6)	W(4)-O(16)	1.950(6)	W(4)-O(28)	2.275(5)
W(4)-O(29)	1.935(6)	W(4)-O(36)	1.920(6)	W(4)-O(39)	1.706(6)
W(5)-O(3)	1.920(6)	W(5)-O(4)	2.270(5)	W(5)-O(7)	1.903(6)
W(5)-O(8)	1.925(6)	W(5)-O(20)	1.957(6)	W(5)-O(35)	1.696(6)
W(6)-O(9)	2.236(6)	W(6)-O(14)	1.878(6)	W(6)-O(27)	1.955(6)
W(6)-O(30)	1.718(6)	W(6)-O(32)	1.975(6)	W(6)-O(33)	1.905(6)
W(7)-O(5)	1.932(5)	W(7)-O(6)	2.291(5)	W(7)-O(11)	1.933(5)
W(7)-O(12)	1.967(6)	W(7)-O(13)	1.694(6)	W(7)-O(29)	1.879(6)
W(8)-O(5)	1.925(5)	W(8)-O(6)	2.242(5)	W(8)-O(17)	1.896(5)
W(8)-O(25)	1.905(6)	W(8)-O(26)	1.718(6)	W(8)-O(34)	1.929(6)
W(9)-O(3)	1.897(5)	W(9)-O(22)	1.921(6)	W(9)-O(24)	1.897(8)
W(9)-O(28)	2.255(5)	W(9)-O(36)	1.929(6)	W(9)-O(40)	1.718(6)
W(10)-O(7)	1.929(6)	W(10)-O(9)	2.256(5)	W(10)-O(18)	1.903(6)
W(10)-O(24)	1.889(6)	W(10)-O(33)	1.961(6)	W(10)-O(38)	1.712(6)
W(11)-O(15)	1.958(6)	W(11)-O(16)	1.899(6)	W(11)-O(21)	1.699(6)
W(11)-O(22)	1.950(6)	W(11)-O(25)	1.909(6)	W(11)-O(28)	2.253(5)

W(12)-O(2)	1.916(6)	W(12)-O(9)	2.272(5)	W(12)-O(11)	1.888(5)
W(12)-O(18)	1.963(6)	W(12)-O(32)	1.930(6)	W(12)-O(37)	1.718(6)
Al(1)-O(4)	1.735(5)	Al(1)-O(6)	1.752(5)	Al(1)-O(9)	1.747(5)
Al(1)-O(18)	1.729(6)	Cu(1)-N(4)	1.902(7)	Cu(1)-N(6)	1.904(7)
Cu(2)-N(1)	1.895(7)	Cu(2)-N(2)	1.890(7)	Cu(3)-N(3)	1.903(7)
Cu(3)-N(5)	1.912(8)	Cu(1)-O(31)	2.315(6)		
O(23)-W(1)-O(4)	168.4(2)	O(23)-W(1)-O(10)	98.0(3)	O(23)-W(1)-O(15)	102.0(3)
O(23)-W(1)-O(17)	101.9(3)	O(23)-W(1)-O(20)	97.8(3)	O(31)-W(2)-O(1)	100.6(3)
O(31)-W(2)-O(6)	169.1(3)	O(31)-W(2)-O(12)	98.4(3)	O(31)-W(2)-O(27)	101.3(3)
O(31)-W(2)-O(34)	97.8(3)	O(19)-W(3)-O(1)	98.8(5)	O(19)-W(3)-O(4)	98.0(4)
O(19)-W(3)-O(8)	169.9(4)	O(19)-W(3)-O(10)	170.1(4)	O(19)-W(3)-O(14)	168.7(4)
O(39)-W(4)-O(2)	100.0(3)	O(39)-W(4)-O(16)	101.1(3)	O(39)-W(4)-O(28)	170.4(3)
O(39)-W(4)-O(29)	102.8(3)	O(39)-W(4)-O(36)	98.1(3)	O(35)-W(5)-O(3)	100.3(3)
O(35)-W(5)-O(4)	170.6(2)	O(35)-W(5)-O(7)	101.3(3)	O(35)-W(5)-O(8)	100.9(3)
O(35)-W(5)-O(20)	98.5(3)	O(30)-W(6)-O(9)	168.7(3)	O(30)-W(6)-O(14)	103.2(3)
O(30)-W(6)-O(27)	99.5(3)	O(30)-W(6)-O(32)	95.8(3)	O(30)-W(6)-O(33)	100.0(3)
O(13)-W(7)-O(5)	98.4(3)	O(13)-W(7)-O(6)	166.9(2)	O(13)-W(7)-O(11)	103.0(3)
O(13)-W(7)-O(12)	97.4(3)	O(13)-W(7)-O(29)	103.8(3)	O(26)-W(8)-O(5)	99.5(3)
O(26)-W(8)-O(6)	170.0(3)	O(26)-W(8)-O(17)	99.8(3)	O(26)-W(8)-O(25)	101.8(3)
O(26)-W(8)-O(34)	98.0(3)	O(40)-W(9)-O(3)	101.7(3)	O(40)-W(9)-O(22)	99.2(3)
O(40)-W(9)-O(24)	100.3(3)	O(40)-W(9)-O(28)	170.5(3)	O(40)-W(9)-O(36)	98.4(3)
O(38)-W(10)-O(9)	101.7(3)	O(38)-W(10)-O(26)	169.2(3)	O(38)-W(10)-O(3)	98.2(3)
O(38)-W(10)-O(27)	101.3(3)	O(38)-W(10)-O(21)	98.0(3)	O(21)-W(11)-O(15)	99.3(3)
O(21)-W(11)-O(16)	101.6(3)	O(21)-W(11)-O(22)	98.2(3)	O(21)-W(11)-O(25)	100.7(3)
O(21)-W(11)-O(28)	171.8(3)	O(37)-W(12)-O(2)	103.1(3)	O(37)-W(12)-O(9)	168.0(3)
O(37)-W(12)-O(11)	102.5(3)	O(37)-W(12)-O(18)	98.0(3)	O(37)-W(12)-O(32)	98.1(3)
O(28)-Al(1)-O(4)	109.7(3)	O(28)-Al(1)-O(6)	109.7(3)	O(28)-Al(1)-O(9)	109.9(3)

2.8 Comparison of the properties of the POMs-based materials with several published supercapacitors

Table S4. Comparison of the properties of the POMs-based materials with several published supercapacitors.

		The capacitances	The cyclic stability	collector	**Ref**
1	Compound **1**	478.41 F g^{-1}(1 A g^{-1})	95.71%(5000 cycles)	carbon cloth	This work
2	Compound **2**	625.99 F g^{-1}(1 A g^{-1})	97.62%(5000 cycles)	carbon cloth	This work
3	$\{Mo_{132}\}$-rGO	617.3 F g^{-1}(5 A g^{-1})	66.7%(3000 cycles)	Ni foams	[3]
4	MWCNT/$Cs_xPMo_{12}O_{40}$	285 F g^{-1}(0.2 A g^{-1})	----		[4]

5	SWCNT/TBA/PMo$_{12}$V$_2$O$_{40}$	444 F g^{-1}(10 mV s^{-1})	95%(6500 cycles)	glassy carbon rods and graphite papers	[5]
6	AC/PW$_{12}$O$_{40}$	254 F g^{-1}(10 mV s^{-1})	35%(30000 cycles)	graphite rods	[6]
7	(H$_2$bpe)(Hbpe)$_2${[Cu(pzta)(H$_2$O)][P$_2$W$_{18}$O$_{62}$]}· 5H$_2$O	168 F g^{-1} (5 A g^{-1})	90.7%(1000 cycles)	glassy carbon	[7]
8	[Ag$_5$(brtmb)$_4$][VW$_{10}$V$_2$O$_{40}$]	206 F g^{-1} (110 A g^{-1})	81.7%(1000 cycles)	glassy carbon	[8]
9	[Cu^{I}(btx)]$_4$[SiW$_{12}$O$_{40}$]	110.3 F g^{-1} (3.0 Ag^{-1})	87%(1000 cycles)	glassy carbon	[9]
10	NENU-5/PPy	779.8 F g^{-1} (10 mV s^{-1})	-----	carbon cloth	[10]
11	[Ag$_5$(C$_2$H$_2$N$_3$)$_6$][H$_5$□SiMo$_{12}$O$_{40}$]@15%GO	230.2 F g^{-1}(0.5 A g^{-1})	92.7%(1000 cycles)	glassy carbon	[11]
12	[H(C$_{10}$H$_{10}$N$_2$)Cu$_2$][PMo$_{12}$O$_{40}$]	287 F g^{-1}(1 A g^{-1})	81.5%(500 cycles)	glassy carbon	[12]
13	[H(C$_{10}$H$_{10}$N$_2$)Cu$_2$][PW$_{12}$O$_{40}$]	153.43F g^{-1}(1A g^{-1})	18.2%(500 cycles)	glassy carbon	[12]
14	[Cu^{I}H$_2$(C$_{12}$H$_{12}$N$_6$)(PMo$_{12}$O$_{40}$)]·[(C$_6$H$_5$N)(H$_2$O)$_2$]	249 F g^{-1}(3 A g^{-1})	93.5%(1000 cycles)	glassy carbon	[13]
15	[Cu$^{II}_2$(C$_{12}$H$_{12}$N$_6$)$_4$(PMo$^{VI}_9$Mo$^{V}_3$O$_{39}$)]	154.5F g^{-1}(3A g^{-1})	91.1%(1000 cycles)	glassy carbon	[13]
16	[Cu$^{I}_4$H$_2$(btx)$_5$(PMo$_{12}$O$_{40}$)$_2$]·2H$_2$O	237 F g^{-1}(2 A g^{-1})	92.5%(1000 cycles)	glassy carbon	[14]
17	[Cu$^{I}_4$H$_2$(btx)$_5$(PW$_1$	100F g^{-1}(2A g^{-1})	90%(1000cycles)	glassy carbon	[14]

	$_2O_{40})_2]\cdot 2H_2O$				
18	$[Cu^{II}Cu^{I}_3(H_2O)_2(btx)_5(PW^{VI}_{10}W^{V}_2O_{40})]\cdot 2H_2O$	82.1F g^{-1}(2A g^{-1})	100%(1000cycles)	glassy carbon	[14]
19	$[Cu^{I}_6(btx)_6(PW^{VI}_9W^{V}_3O_{40})]\cdot 2H_2O$	76.4F g^{-1}(2A g^{-1})	100%(1000cycles)	glassy carbon	[14]
20	$[Cu^{II}Cu^{I}_3(btx)_5(SiMo^{VI}_{11}Mo^{V}O_{40})]\cdot 4H_2O$	138.4F g^{-1}(2A g^{-1})	97%(1000cycles)	glassy carbon	[14]
21	$[\{Ag_5(pz)_7\}(BW_{12}O_{40})]$	1058 F g^{-1}(2.16 A g^{-1})	90.3%(1000 cycles)	glassy carbon	[15]
22	$[\{Ag_5(pz)_7\}(SiW_{12}O_{40})](OH)\cdot H_2O$	986F g^{-1}(2.16A g^{-1})	94.5%(1000 cycles)	glassy carbon	[15]
23	(Hpyr)$[\{Ag(pz)\}_2(PMo_{12}O_{40})$	1611F g^{-1}(2.16A g^{-1})	84.8%(1000 cycles)	glassy carbon	[15]
24	$[Cu^{I}_3(pz)_2(phen)_3]_2[Cu^{I}(phen)_2][\{Na(H_2O)_2\}\{(V^{IV}_5Cu^{II}O_6)(As^{III}W_9O_{33})_2\}]\cdot 6H_2O$	825 F g^{-1}(2.4 A g^{-1})	91.4%(3000 cycles)	glassy carbon	[16]
25	$[Cu^{I}_2(bnie)_2]_2(\beta\text{-}Mo_8O_{26})$	828F g^{-1}(1A g^{-1})	100%(5000 cycles)	nickel foam	[17]
26	$[Cu^{I}_2(\beta\text{-}Mo_8O_{26})(bnie)_2][Cu_2(bnie)_2]$	800F g^{-1}(1A g^{-1})	-----	nickel foam	[17]
27	Pinecone	361 F g^{-1}	-----	titanium foil	[18]

	AC/$PMo_{12}O_{40}$				
28	RGO/PIL/ $PMo_{12}O_{40}$	408 F g^{-1}	98% (2000 cycles)	stainless steel foil	[19]
29	RGO/$PMo_{12}O_{40}$	276 F g^{-1}	96% (10000 cycles)	Graphite roods	[20]
30	RGO/ $PMo_{12}O_{40}$	51.2 F g^{-1}	95% (5000 cycles)	commercial flexible carbon cloth	[21]
31	AC/$PMo_{12}O_{40}$	136 F g^{-1}	91% (8000 cycles)		[22]
32	AC/$PMo_{12}O_{40}$	223F g^{-1}	100% (10000 cycles)	Ti foils	[23]
33	AC/$PMo_{12}O_{40}$	293F g^{-1}	-----	C250 carbon monoliths	[24]
34	PAni/$H_3PMo_{12}O_{40}$	120F g^{-1}	70% (1000 cycles)	Rigid graphite plate	[25]
35	$[Ag_5(brtmb)_4][VW_{10}V_2O_{40}]$	206 F g^{-1}(110 A g^{-1})	81.7%(1000 cycles)	glassy carbon	[26]
36	rGO-PMo_{12}	278 mF cm^{-2}	89%(5000 cycles)	Carbon cloth	[27]
37	AC/P_2Mo_{18}	275F g^{-1}(6A g^{-1})	89%(2000 cycles)	The stainless steel wire mesh	[28]
38	VSM/CNW	1962F g^{-1}(1A g^{-1})	97%(1200 cycles)	nickel foam	[29]
39	$[Ag_5(C_2H_2N_3)_6][H_5SiMo_{12}O_{40}]$@15% GO-based electrode	230.2F g^{-1}(0.5A g^{-1})	92.7%(1000cycles)	glassy carbon	[30]

2.9 Comparison of the properties of the POMs-based materials with several published H_2O_2 sensors

Table S5. Comparison of the properties of the POMs-based materials with several published H_2O_2 sensors.

Electrode material	Potential (V)	Linear range	detection limit	Ref.
Compound 1	-0.5 V	1.20-3.20mM	0.93μM	This work
Compound 2	-0.5 V	19.95μM-0.90mM	0.86μM	This work
{PEI/[$P_2W_{17}Fe$/PEI-PdNPs]/$P_2W_{17}Fe$}$_3$	-0.2V	1.5μM-3.9 mM	1 μM	[31]
{PEI/(P_8W_{48}/chitosan)$_8$}	-0.8V	2.5×10^{-5}-2.3 $\times10^{-3}$ M	1.3 μM	[32]
[PB/WV-Pt@Pd]$_6$/ITO	-0.3V	0.4–2650μM	1.00 $\times10^{-7}$ M	[33]
$H_4PW_{18}O_{62}$/GC	−0.4V	5.0×10^{-4} to 9.0×10^{-2} M	0.5μM	[34]
P_2Mo_{18}/GC	0V	1.6×10^{-4} to 4.4×10^{-2} M	53.4μM	[35]
P_2W_{18}/GC	-0.4V	Up to 0.4×10^{-3}M	---	[36]
$SiMo_9W_2$/ITO	-0.4V	Up to 3.2×10^{-2}M	---	[37]
$P_2W_{17}V$/CCE	-0.435V	1×10^{-4} to 2×10^{-2} M	40μM	[38]
$PFeW_{11}$/CPE	0V	1×10^{-5} to 2×10^{-4} M	7.4μM0	[39]
[Cu_2(bep)(ada)$_2$]H_2O}$_n$	-0.45V	0.05-3μM	0.014μM	[40]
MIL-53-Cr^{III}As/GCE	-0.38V	25-500μM	3.52μM	[41]
MWCNTs/[C_8Py][PF_6]-PMo_{12}	-0.1V	0.02-8mM	12μM	[42]
$[PFeW_{11}O_{39}]^{-4}$	-0.04V	9	---	[43]

PMo_{12}-PPy	0.18V	0.2-30	50μM	[44]
$Na_2H_6CoW_{11}Co(H_2O)O_{39}$	-0.5V	---	---	[45]
SWCNTs/$[SiMo_{12}O_{40}]^{4-}$	0.08V	(10-18) × 10^{-3}	0.5μM	[46]
PMo_{12}	0V	0.02-30mM	7μM	[47]
P_2Mo_{18}	0.35V	Down to 10mM	---	[48]
PVW_{11}	-0.5	Up to 26.4mM	---	[49]
PMo_{12}	0.05	2-15mM	---	[50]

3. References

[1] T. S. Natarajan, M. Thomas, K. Natarajan, H. C. Bajaj, R. J. Tayade,Study on UV-LED/TiO_2 process for degradation of Rhodamine B dye, *Chem. Eng J.*, 2011, **169**, 126-134.DOI: 10.1016/j.cej.2011.02.066

[2] J. J. Ma, L. C. Zhou, W. F. Dan, H. Zhang,Y. M. Shao,C. Bao,L. Y. Jing. Novel magnetic porous carbon spheres derived from chelating resin as a heterogeneous Fenton catalyst for the removal of methylene blue from aqueous solution, *J Colloid Interf Sci*, 2015, **446**, 298–306. DOI:10.1016/j.jcis.2015.01.036

[3] Y. N. Dong, L. Chen, W. L. Chen, X. T .Zheng, X. L. Wang, E. B. Wang, Keplerate-type Polyoxometalate with Large Electronegativity Functionalized rGO for High-Energy Density Aqueous Asymmetric Supercapacitors, *Chem-Asian J*, 2018, **13**, 3304-3313. DOI: 10.1002/asia.201801018

[4] A. K. C. Gallegos, R. M. Rosales, M. Baibarac, P. G. Romero, M. E. Rincón, Electrochemical supercapacitors based on novel hybrid materials made of carbon nanotubes and polyoxometalates, *Electrochem Commun*, 2007, **9**, 2088–2092.DOI:10.1016/j.elecom.2007.06.003

[5] H. Y. Chen, R. A. Oweini, J. Friedl, C. Y. Lee, L. L. Li, U. Kortz, U. Stimming and M Srinivasan, A novel SWCNT-polyoxometalate nanohybrid material as an electrode for electrochemical supercapacitors, *Nanoscale*, 2015, **7**, 7934-7941. DOI:10.1039/c4nr07528e

[6] J. S. Guevar,V. Ruiz, P. G. Romero, Hybrid energy storage: high voltage aqueous supercapacitors based on activated carbon-phosphotungstate hybrid materials, *J. Mater. Chem. A*, 2014, **2**,1014-1021.DOI:10.1039/c3ta14455k

[7] G. N. Wang, T. T. Chen, S. B. Li, H. J. Pang, H. Y. Ma, A coordination polymer based on dinuclear (pyrazinyl tetrazolate) copper(II) cations and Wells-Dawson anions for high-performance supercapacitor electrodes, *Dalton Trans*, 2017,**46**,13897-13902. DOI:10.1039/C7DT02230A

[8] G. N. Wang, T. T. Chen, X. M. Wang, H. Y. Ma, H. J. Pang, A High-Performance Supercapacitor Afforded by a High-Connected Keggin based 3D Coordination Polymer, *Eur J inorg Chem*, 2017, **45**, 5350-5355. DOI: 10.1002/ejic.201701031

[9] D. F. Chai, Y. Hou, K. P. O'Halloran, H. J. Pang, H. Y. Ma, G. N. Wang, X. M. Wang, Enhancing Energy Storage via TEA-Dependent Controlled Syntheses: Two Series of Polyoxometalate-Based Inorganic-Organic Hybrids and their Supercapacitor Properties, *Chem Electro Chem*, 2018,**5**, 3443-3450. DOI: 10.1002/celc.201801081

[10] H. N. Wang, M. Zhang, A. M. Zhang, F. C. Shen, X. K. Wang, S. N. Sun, Y. J. Chen, Y. Q. Lan, Polyoxometalate-Based Metal-Organic Frameworks with Conductive Polypyrrole for Supercapacitors, *ACS Appl. Mater. Interfaces*, 2018, **10**, 32265-32270. DOI: 10.1021/acsami.8b12194

[11] Y. Hou, D. F. Chai,B. N. Li, H. J. Pang, H. Y. Ma, X. M. Wang, L. C. Tan, Polyoxometalate-Incorporated Metallacalixarene@Graphene Composite Electrodes for High-Performance Supercapacitor, *ACS Appl. Mater. Interfaces*, 2019,**11**,20845-20853. DOI: 10.1021/acsami.9b04649

[12] S. Roy, V. Vemuri, S. Maiti, K. S. Manoj, U. Subbarao, and S. C. Peter, Two Keggin-Based Isostructural POMOF Hybrids: Synthesis, Crystal Structure, and Catalytic Properties, *Inorg. Chem.*, 2018, **57**,12078-12092. DOI: 10.1021/acs.inorgchem.8b01631

[13] D. F. Chai, J. J. Xin, B. N. Li, H.J. Pang, H. Y. Ma, K. Q. Li, B. X. Xiao, X. M. Wanga and L. C. Tana, Mo-based crystal POMOFs with high electrochemical capacitor performance, Dalton Trans., 2019, **48**, 13026-13033. DOI:10.1039/C9DT02420D

[14] D. F. Chai, Carlos J. Gómez-García, B. N. Li, H. J. Pang, H. Y. Ma, X. M. Wang , and L. C. Tan, Polyoxometalate-based metal-organic frameworks for boosting electrochemical capacitor performance, *Chem Eng J*, 2019,**373**,587-597. DOI:10.1016/j.cej.2019.05.084

[15] N. N. Du, L. G. Gong, L. Y. Fan, K. Yu, H. Luo, S. J. Pang, J. Q. Gao, Z. W. Zheng, J. H. Lv,and B. B. Zhou, Nanocomposites Containing Keggin Anions Anchored on Pyrazine Based Frameworks for Use as Supercapacitors and Photocatalysts, *ACS Appl. Nano Mater*, 2019, **2**, 3039-3049. DOI: 10.1021/acsanm.9b00409

[16] K. P. Wang, K. Yu, J. H. Lv, M. L. Zhang, F. X. Meng, and B. B. Zhou, A Host−Guest Supercapacitor Electrode Material Based on a Mixed Hexa-Transition Metal Sandwiched Arsenotungstate Chain and Three-Dimensional Supramolecular Metal−Organic Networks with One-Dimensional Cavities, *Inorg. Chem.*, 2019,**58**,7947-7957. DOI: 10.1021/acs.inorgchem.9b00692

[17] L. G. Devi , S. G. Kumar , K. M. Reddy ,C. Munikrishnappa, Photo degradation of methyl orange an azo dye by advanced Fenton process using zero valent metallic iron: influence of various reaction parameters and its degradation mechanism, *J Hazard Mater*, 2008,**164**, 459-467. DOI: 10.1016/j.jhazmat.2008.08.017

[18] M. Genovese and K. Lian, Polyoxometalate Modified Pine Cone Biochar Carbon for Supercapacitor Electrodes, *J. Mater. Chem. A*, 2017,**5**, 3939-3947. DOI: 10.1039/C6TA10382K

[19] M. H. Yang, B. G. Choi, S. C. Jung, Y. K. Han, Y. S. Huh, S. B. Lee, Polyoxometalate-coupled Graphene via Polymeric Ionic Liquid Linker for Supercapacitors, *Adv. Funct. Mater.* 2014, **24**, 7301-7309.DOI:10.1002/adfm.201401798

[20] J. S.Guevara, V. Ruiza and P. G. Romero, Stable graphene-polyoxometalate nanomaterials for application in hybrid supercapacitors, *Phys. Chem. Chem. Phys.*, 2014, **16**, 20411-20414. DOI:10.1039/C4CP03321C

[21] D. P. Dubal, J. S.Guevara, D. Tonti, E. Encisoc and P. G. Romero, A high voltage solid state symmetric supercapacitor based on graphene-polyoxometalate hybrid electrodes with a hydroquinone doped hybrid gel-electrolyte, *J. Mater. Chem. A*, 2015, **3**, 23483-23492. DOI: 10.1039/C5TA05660H

[22] V.Ruiz, J. S. Guevara, P.G. Romero, Hybrid electrodes based on polyoxometalate-carbon materials for electrochemical supercapacitors, *Electrochem Commun*, 2012, **24**, 35-38.DOI:10.1016/j.elecom.2012.08.003

[23] C. C. Hu,E. B. Zhao, N.Nitta, A. Magasinski,G. Berdichevsky, G.Yushin, Aqueous solutions of acidic ionic liquids for enhanced stability of polyoxometalate-carbon supercapacitor electrodes, *J Power Sources*, 2016, **326**, 569-574.DOI:10.1016/j.jpowsour.2016.04.036

[24] P. Palomino, J. S. Guevara,M. O. Marínc, V. Ruiz, D. P. Dubal, P. G.Romero, D.Tonti, E.Enciso, Influence of texture in hybrid carbon-phosphomolybdic acid materials on their performance as electrodes in supercapacitors, *Carbon*, 2017, **111**, 74-82. DOI: 10.1016/j.carbon.2016.09.054

[25] A. K. C. Gallegos, M. L. Cantú, N. C. Pastor, P. G. Romero,Nanocomposite Hybrid Molecular Materials for Application in Solid-State Electrochemical Supercapacitors, *Adv. Funct. Mater*. 2005 , **15** , 1125-1133. DOI:https://doi.org/10.1002/adfm.200400326

[26] G. N. Wang, T. T. Chen, X. M. Wang, H. Y. Ma, H. J. Pang, High-Performance Supercapacitor Afforded by a HighConnected Keggin-Based 3D Coordination Polymer, *Eur. J. Inorg. Chem.*, 2017, 5350-5355. DOI:10.1002/ejic.201701031

[27] D. P. Dubal, N. R. Chodankar, A. Vinu, D. H. Kim, P. Gomez-Romero,Asymmetric Supercapacitors Based on Reduced Graphene Oxide with Different Polyoxometalates as Positive and Negative Electrodes, *ChemSusChem*, 2017, **10**, 2742-2750. DOI: 10.1002/cssc.201700792

[28] A. Mu, J. S. Li, W. L. Chen, X. J. Sang, Z. M. Su, E. B. Wang, The composite material based on Dawson-type polyoxometalate and activated carbon as the supercapacitor electrode, *Inorg. Chem. Commun.*, 2015, **46**, 149-152. DOI: 10.1016/j.inoche.2015.03.032

[29] T. Deng, W. Zhang, O. Arcelus, D. Wang, X. Y. Shi, X. Y. Zhang, J. Carrasco, T. Rojo, W. T. Zheng, Vertically co-oriented two dimensional metalorganic frameworks for packaging enhancedsupercapacitive performance,*Commun. Chem.*, 2018,**1**,1- 6.DOI:10.1038/s42004-017-0005-1

[30] Y. Hou, D. F. Chai, B. N. Li, H. J. Pang, H. Y. Ma, X. M. Wang, L. C. Tan, Polyoxometalate-Incorporated Metallacalixarene@Graphene Composite Electrodes for High-Performance Supercapacitor, ACS Appl. Mater. Interfaces, 2019, **23**, 20845-20853.DOI:10.1021/acsami.9b04649

[31] H. Y. Ma, Z. J. Zhang, H. J. Pang, S. Li, Y. Y. Chen, W. J. Zhang, Fabrication and electrochemical sensing property of a composite film based on a polyoxometalate and palladium nanoparticles, *Electrochimica Acta*, 2012, **69** ,379-383. DOI:10.1016/j.electacta.2012.03.017

[32] L. Kang, H. Y. Ma, Y. Yu, H. J. Pang, Y. B. Song, D. Zhang, Study on amperometric sensing performance of a crown-shaped phosphotungstate-based multilayer film, *Sensors Actuat B-Chem*, 2013, **177**, 270-278.DOI:10.1016/j.snb.2012.10.126

[33] D. Zhu, J. W. Zuo, L. C. Tan, H. J. Pang and H. Y. Ma, Enzymeless electrochemical determination of hydrogen peroxide at a heteropolyanion-based composite film electrode, *New J. Chem.*, 2019, **43**, 1053-1062. DOI:10.1039/c8nj04570d

[34] M. Ammam, E.B. Easton, Novel organic–inorganic hybrid material based on tris(2,2-bipyridyl)dichlororuthenium(II) hexahydrate and Dawson-type tungstophosphate $K_7[H_4PW_{18}O_{62}]\cdot 18H_2O$ as a bifunctional hydrogen peroxide electrocatalyst for biosensors, *Sensor Actuat B-Chem*, 2012, **161**,520–527. DOI:10.1016/j.snb.2011.10.070

[35] M. Zhou, L.P. Guo, F.Y. Lin, H.X. Liu, Electrochemistry and electrocatalysis of polyoxometalate-ordered mesoporous carbon modified electrode, *Anal Chim Acta*, 2007, **587**, 124–131. DOI:10.1016/j.aca.2007.01.017

[36] N. Fay, E. Dempsey, T. McCormac, Assembly, electrochemical characterisation and electrocatalytic ability of multilayer films based on $[Fe(bpy)_3]^{2+}$, and the Dawson heteropolyanion,$[P_2W_{18}O_{62}]^{6-}$, *J Electroanal Chem*, 2005, **574**, 359-366. DOI:10.1016/j.jelechem.2004.07.038

[37] T. Dong, H. Y. Ma, W. Zhang, L. H. Gong, F. P. Wang, C. X. Li, Electrochemical behavior and luminescent properties of a multilayer film containing mixed-addenda polyoxometalates $K_{10}H_3[Eu(SiMo_9W_2O_{39})_2]$ and tris(2,2-bipyridine)ruthenium(II), *J Colloid Interf Sci*, **2007**, **311**,523–529. DOI:10.1016/j.jcis.2007.03.014

[38] P. Wang, X. Q. Wang, L.H. Bi, G.Y. Zhu, Sol–gel-derived α_2-$K_7P_2W_{17}VO_{62}$: graphite: organoceramic composite as the electrode material for a renewable amperometric hydrogen peroxide sensor, *J Electroanal Chem*, 2000, **495**,51–56. DOI：10.1016/S0022-0728(00)00371-5

[39] H. Hamidia, E. Shamsb, B. Yadollahi, F.K. Esfahani, Fabrication of carbon paste electrode containing $[PFeW_{11}O_{39}]^{4-}$ polyoxoanion supported on modified amorphous silica gel and its electrocatalytic activity for H_2O_2 reduction, *Electrochimica Acta*, 2009, **54**, 3495–3500. DOI:10.1016/j.electacta.2008.12.063

[40] W. Meng, S. Xu, L. Dai, Y. Li, J. Zhu and L. Wang, An enhanced sensitivity towards H_2O_2 reduction based on a novel Cu metal–organic framework and acetylene black modified electrode, *Electrochim. Acta*, **2017**, **230**, 324–332.DOI: 10.1016/j.electacta.2017.02.017

[41] N. S. Lopa, M. M. Rahman, F. Ahmed, S. Chandra Sutradhar, T. Ryu and W. Kim,A base-stable metal-organic framework for sensitive and non-enzymatic electrochemical detection of hydrogen peroxide, *Electrochim. Acta*, 2018, **274**, 49–56.DOI:10.1016/j.electacta.2018.03.148

[42] B. Haghighi, H. Hamidi, L. Gorton, Formation of a robust and stable film comprising ionic liquid and polyoxometalate on glassy carbon electrode modified with multiwalled carbon nanotubes: toward sensitive and fast detection of hydrogen peroxide and iodate, *Electrochim. Acta*, 2010, **55**, 4750-4757. DOI:10.1016/j.electacta.2010.03.041

[43] S. Gaspar, L. Muresan, A. Patrut, I.C. Popescu, $PFeW_{11}$-doped polymer film modified electrodes and their electrocatalytic activity for H_2O_2 reduction, *Anal.Chim. Acta*, 1999, **385**, 111-117.DOI:10.1016/S0003-2670(98)00784-3

[44] X. Wang, H. Zhang, E. Wang, Z. Han, C. Hu, Phosphomolybdate-polypyrrole composite bulk-modified carbon paste electrode for a hydrogen peroxide amperometric sensor, *Mater. Lett.*, 2004, **58**, 1661-1664.DOI:10.1016/j.matlet.2003.10.044

[45] Y. Li, W. Bu, L. Wu, C. Sun, A new amperometric sensor for the determination of bromate, iodate and hydrogen peroxide based on titania sol-gel matrix for immobilization of cobalt substituted Keggin-type cobalttungstate anion by vapor deposition method, *Sens. Actuators B*, 2005, **107**, 921-928.

DOI:10.1016/j.snb.2004.12.040

[46] A. Salimi, A. Korani, R. Hallaj, R. Khoshnavazi, H. Hadadzadeh, Immobilization of $[Cu(bpy)_2]Br_2$ complex onto a glassy carbon electrode modified with alpha-$SiMo_{12}O_{40}^{4-}$ and single walled carbon nanotubes: application to nanomolar detection of hydrogen peroxide and bromate, *Anal. Chim. Acta*, 2009, **635**, 63-70.DOI:10.1016/j.aca.2009.01.007

[47] W. Song, Y. Liu, N. Lu, H. Xu, C. Sun, Application of the sol-gel technique to polyoxometalates: towards a new chemically modified electrode, *Electrochim. Acta*, 2000, **45**,1639-1644.DOI:10.1016/S0013-4686(99)00326-6

[48] D. Martel, A. Kuhn, Electrocatalytic reduction of H_2O_2 at $P_2Mo_{18}O_{62}^{6-}$ modified glassy carbon, Electrochim. Acta, 2000, **45** ,1829-1836. DOI:10.1016/S0013-4686(99)00399-0

[49] C. Li, R. Cao, K.P. O'Halloran, H. Ma, L. Wu, Preparation, characterization and bifunctional electrocatalysis of an inorganic-organic complex with a vanadium-substituted polyoxometalate, *Electrochim. Acta*, 2008, **54** , 484-489. DOI:10.1016/j.electacta.2008.07.039

[50] A. Z. Ernst, S. Zoladek, K. Wiaderek, J. A. Cox, A. Kolary-Zurowska, K. Miecznikowski, P.J. Kulesza,Network films of conducting polymer-linked polyoxometalate-modified gold nanoparticles: Preparation and electrochemical characterization, Electrochim. Acta, 2008, **53**, 3924-3931. DOI: 10.1016/j.electacta.2007.12.053